Environmental Science: Atmospheres

ROYAL SOCIETY OF CHEMISTRY

PAPER

View Article Online
View Journal | View Issue

Cite this: *Environ. Sci.: Atmos.*, 2026, **6**, 579

Quantification, diel variation and photochemistry of inorganic chlorine trace gases in continental Germany

Lasse Moormann, *[a] John N. Crowley, [b] Friederike Fachinger[a] and Frank Drewnick[a]

Understanding the sources, distribution, and lifetime of inorganic chlorine-containing trace gases is crucial to assessing their tropospheric impacts. We report *in situ* measurements of Cl_2, HOCl, $ClNO_2$, and $ClONO_2$ using iodide chemical ionization mass spectrometry during a 2.5-week campaign in June 2024 at a rural continental site in central Germany. Air masses that had passed over "marine-anthropogenic" regions (≈400 km distant) showed significantly higher mixing ratios of chlorine-containing gases than "continental-unpolluted" air masses. From the marine-anthropogenic period, we provide the first quantitative observations of $ClONO_2$ in the lower troposphere (up to 59.8 pptv during daytime). Persistent nonzero $ClONO_2$ at night implies a non-photochemical source of $ClONO_2$ or its precursor ClO, and/or that heterogeneous loss is slower than laboratory uptake coefficients suggest. $ClNO_2$ levels were consistent with production *via* N_2O_5 uptake on chloride-containing particles; both $ClNO_2$ and Cl_2 were enhanced when O_3-/N_2O_5-rich air entrained into the nocturnal boundary layer. Photolysis of $ClNO_2$, Cl_2, and HOCl yielded mean maximum Cl atom production rates of 1.0×10^6 cm^{-3} s^{-1} under marine-anthropogenic influenced air and 1.6×10^5 cm^{-3} s^{-1} under continental-unpolluted conditions. In the early morning, Cl production (due to $ClNO_2$ photolysis) exceeded primary–OH production from O_3 photolysis, while after noon HOCl photolysis was the dominant Cl source. At low solar zenith angles, HOCl photolysis contributed up to 40% of primary OH. These measurements indicate that Cl atoms can strongly influence hydrocarbon oxidation in similar rural regions, with potential regional and global implications (of up to 15%) for the methane lifetime.

Received 27th October 2025
Accepted 2nd February 2026

DOI: 10.1039/d5ea00142k

rsc.li/esatmospheres

Environmental significance

Tropospheric, inorganic chlorine-containing trace gases (Cl-species) provide a source of chlorine atoms that impact *e.g.* on the rates of hydrocarbon oxidation and thus photochemical O_3 formation. We report measurements of Cl_2, $ClNO_2$, $ClONO_2$ and HOCl in central Germany, distant from coastal regions and thus not expected to be influenced by marine-emissions of sea-salt. The measurement of $ClONO_2$, the first ever made in the lower troposphere, enabled estimation of nighttime ClO and Cl radical mixing ratios. The impact of Cl_2, $ClNO_2$, $ClONO_2$ and HOCl on Cl and OH radical production is shown to be significant in rural continental regions, when air masses have passed marine and anthropogenically polluted regions. Further estimations suggest a significant influence on the methane lifetime.

1 Introduction

The role of inorganic chlorine trace-gases in atmospheric science is well established for the stratosphere, where molecules such as $ClONO_2$, HOCl, HCl and thermally unstable Cl_2O_2 play a central role in ozone depletion, most noticeably in polar regions where the catalytic recycling of Cl atoms through a mixture of heterogeneous and photochemical processes leads to the formation of the "ozone-hole".[1–3] In the stratosphere, the source of reactive chlorine trace gases is the photolysis of organic chlorine-containing species such as CH_3Cl and CCl_2F_2, which were emitted into the lower atmosphere in large quantities prior to their ban in the Montreal Protocol in 1989.[4–7]

Chlorine species are highly reactive when in radical forms such as Cl or ClO, resulting in a short lifetime (seconds) and significant chemical effects on their immediate environment. The lifetime of the inorganic radical reservoirs, including photolabile Cl_2, $ClNO_2$, $ClONO_2$, and HOCl depends on the actinic flux,[8,9] while the lifetime of HCl depends on its reaction with OH and deposition. While there are several observations of $ClNO_2$, HOCl, and Cl_2 in the troposphere *e.g.*,[10–14] $ClONO_2$ is considered

[a]*Multiphase Chemistry Department, Max Planck Institute for Chemistry, Mainz, 55128, Germany. E-mail: lasse-moormann@mpic.de*

[b]*Atmospheric Chemistry Department, Max Planck Institute for Chemistry, Mainz, 55128, Germany*

as a stratospheric trace gas, which is only present in the upper troposphere as a result of intrusion from stratospheric air masses.[15–17] In the troposphere, chlorine atoms are important as they contribute significantly to the oxidative capacity and especially the oxidation of hydrocarbons.[18–21]

The presence of chlorine radicals derived from inorganic reservoirs such as $ClNO_2$ and HOCl enhances the rate of oxidation of hydrocarbons (forming HCl and organic peroxyl radicals), which influences air composition and especially photochemical ozone production.[22–24] Understanding the sources, distribution and lifetime of inorganic chlorine trace-gases is thus crucial for evaluating their impact on chemical processes in the troposphere.

$ClNO_2$ and Cl_2, HOCl and HCl (in both gas and particle phases) are generally believed to be the most abundant, inorganic chlorine-containing gas phase species in the troposphere.[25] Various routes to their formation in the atmosphere are illustrated in Fig. 1 and described below.

The main source of gaseous inorganic chlorine in the troposphere is the release in the form of HCl, *e.g.*, *via* acid displacement of chloride from sea-salt (mainly NaCl)[26–28] and gaseous emission from biomass burning, waste disposal, and fossil fuel extraction.[29–33] Additionally, HCl can be formed through H-abstraction from volatile organic compounds (VOCs) by Cl atoms that originate from the mechanisms discussed below.[25] In a continental atmosphere, NH_3 and HCl react to form NH_4Cl, which partially partitions into the particle phase. The heterogenous uptake of N_2O_5 on chlorinated particles, liberates chloride as $ClNO_2$ into the gas phase.[34]

$$N_2O_5 + Cl^- \rightarrow ClNO_2 + NO_3^- \quad (R1)$$

N_2O_5 is formed in the reaction between NO_2 and NO_3 (the latter formed in the oxidation of NO_2 by O_3) and, due to its thermal equilibrium with photolabile NO_3 (R2), is only present in significant concentrations at night:[35]

$$NO_2 + NO_3 + M \leftrightarrow N_2O_5 + M \quad (R2)$$

The abundance of N_2O_5 (and thus $ClNO_2$) is closely tied to the availability of NO_X and the lifetime of NO_3 and is therefore maximized in nocturnal air masses that are either impacted by anthropogenic emissions with high levels of NO_X or in which the NO_3 reactivity towards unsaturated hydrocarbons is low. NO_3 and thus N_2O_5 lifetimes in forested regions are often very short[36,37] as the abundance of terpenoids, which react rapidly with NO_3, is high. In this case, activation of reactive chlorine from its particle reservoirs is inefficient and the formation of $ClNO_2$ is suppressed. High levels of $ClNO_2$ are typically found at night in polluted marine areas such as Asian megacities and industrial metropolitan areas.[38–41] $ClNO_2$ has also been observed in air masses which have been transported long distances from polluted and marine source regions to continental sites.[10,13,14]

Once formed in the multiphase reaction between N_2O_5 and particle-chloride, most of the $ClNO_2$, which has a low solubility,[42] is released into the gas phase where it is photolyzed to Cl and NO_2 (R3).[43–45] Other loss processes, such as reaction with OH are negligible by comparison.[46]

$$ClNO_2 + h\nu \rightarrow Cl + NO_2 \quad (R3)$$

$ClNO_2$ can also react with acidified (pH < 2), chloride-containing particles to generate gas-phase Cl_2:

$$ClNO_2 + Cl^- \rightarrow Cl_2 + NO_2^- \quad (R4)$$

Cl_2 is also formed through the uptake of O_3 onto acidic, chloride-containing particles[30] and (as shown below) through other heterogeneous processes.[47] During daytime, Cl_2 is rapidly photolyzed in the troposphere (lifetime ~10 min) to form two Cl atoms:

$$Cl_2 + h\nu \rightarrow 2Cl \quad (R5)$$

The ClO radical is formed when Cl atoms react with O_3 (R6).[34] ClO radicals then react with HO_2 and NO_2 to form HOCl and $ClONO_2$, respectively ((R7) and (R8)).

$$Cl + O_3 \rightarrow ClO + O_2 \quad (R6)$$

$$ClO + HO_2 \rightarrow HOCl + O_2 \quad (R7)$$

$$ClO + NO_2 + M \rightarrow ClONO_2 + M \quad (R8)$$

As HO_X radicals are ubiquitous in the atmosphere, the ClO radical is the limiting trace gas for formation of HOCl. Consequently, larger mixing ratios of the latter have been measured near source regions with high chloride load such as marine sites or industrial facilities.[11,48] The formation of $ClONO_2$ requires the presence of NO_2 and is thus expected to be formed at largest rates in regions with both anthropogenic influence and particulate chloride as precursor for Cl-atoms and thus ClO.

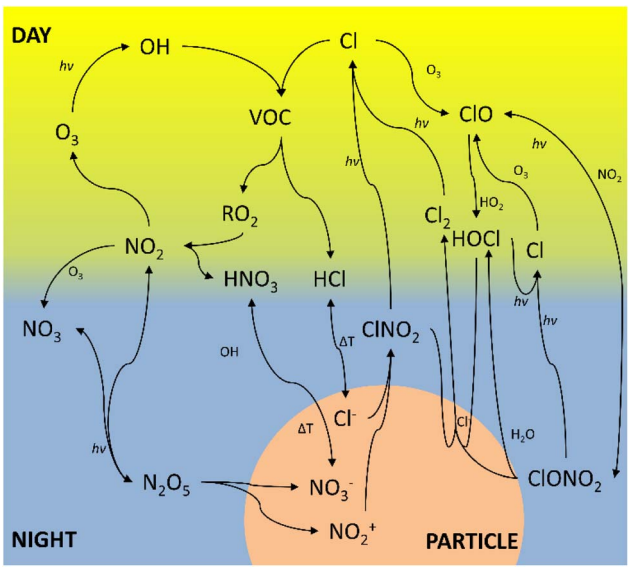

Fig. 1 A simplified diagram for formation and (photo)chemical transformations of chlorine-containing trace-gases in the troposphere. The links to NO_Y (*e.g.*, NO_2, NO_3 and N_2O_5) are highlighted, as is the coupling with HO_X cycles (OH and HO_2).

HOCl and $ClONO_2$ are lost in both gas- and multiphase processes. Similar to $ClNO_2$, the uptake of HOCl or $ClONO_2$ to chloride-containing, acidic particles results in the generation of Cl_2 ((R9) and (R10)),[49,50] while heterogenous hydrolysis of $ClONO_2$ forms HOCl (R11).[51] The photolysis of HOCl leads to the production of Cl atoms and OH radicals (R12), whereas the photolysis of $ClONO_2$ leads mainly to Cl atoms (R13a) with a minor contribution to ClO formation (R13b).[34]

$$HOCl + Cl^- \rightarrow Cl_2 + OH^- \quad (R9)$$

$$ClONO_2 + Cl^- \rightarrow Cl_2 + NO_3^- \quad (R10)$$

$$ClONO_2 + H_2O \rightarrow HOCl + HNO_3 \quad (R11)$$

$$HOCl + h\nu \rightarrow Cl + OH \quad (R12)$$

$$ClONO_2 + h\nu \rightarrow Cl + NO_3 \quad (R13a)$$

$$ClONO_2 + h\nu \rightarrow ClO + NO_2 \quad (R13b)$$

Measurements of chlorine-containing trace-gases in the troposphere date back to the mid-1980s, whereby chromatographic methods were used to monitor *e.g.*, HCl and HOCl.[26,52] Recent developments in mass spectrometry have enabled sensitive and selective detection of several chlorinated trace gases with chemical-ionization mass spectrometry (CIMS) using iodide as the reagent ion for a wide variety of inorganic chlorine species.[11,23,53,54] The recent development of high-resolution (*e.g.*, Time-of-Flight, ToF) analysers allows identification of non-fragmented chlorine species and therefore offers high selectivity as well as excellent sensitivity. However, the number of studies using such devices to examine tropospheric chlorine chemistry is still limited and those available mostly report measurements in polluted marine regions. The presence of chlorine-species in rural continental sites, where the source of chlorine is obscure, remains largely unexplored.

In this study we present the quantitative measurement of Cl_2, HOCl, $ClNO_2$ and $ClONO_2$ using VUV-Iodide-ToF-CIMS during field measurements in central Germany. The formation and loss of inorganic chlorine-containing species throughout the diel cycle are discussed, including the first quantitative measurements of $ClONO_2$ in the troposphere and potential limitations by interfering secondary ion reactions. The goal of our analysis is to assess the influence of chlorine species on local Cl and OH production for air masses with marine-anthropogenic and continental-unpolluted origin and to estimate the impact on *e.g.*, the lifetimes of methane and non-methane hydrocarbons.

2 Methods: CIMS operation and calibration

The inorganic chlorine trace-gases $ClNO_2$, $ClONO_2$, HOCl and Cl_2 as well as N_2O_5 were measured using an Iodide-ToF-CIMS (Aerodyne Research Inc., USA[55]) during the BISTUM24 campaign (Section 2.3) and in further laboratory studies (Section 2.2 and Supplement). A vacuum ultraviolet (VUV) lamp and 20 ppmv CH_3I in N_2 were used to generate iodide primary ions, which form clusters with the inorganic chlorine-containing compounds in the ion molecular reactor (IMR). The IMR was maintained at 170 mbar, heated to 60 °C and continuously humidified (>7000 ppm H_2O). The chlorine-containing trace gases and N_2O_5 were detected as clusters with iodide at the mass-to-charge ratios (m/z) listed in Table 1. During all measurements, the CIMS resolution was $m/z/\Delta m/z = 5000$ at m/z 250. Peak assignment and data processing was conducted with Tofware V4.0.3, ensuring that isotopic ratios are in accordance with their natural abundance. Iodide clusters with Cl and ClO were also observed but were minor in magnitude (<3%) of the signal from $ClNO_2$. These were excluded from further analysis as they most likely originate from the fragmentation of larger chlorine-containing species[39] as indicated by high correlations with $ClNO_2$ ($R^2 = 0.96$). The unambiguous first in-field detection of $ClONO_2$ is shown in the mass spectra in Fig. S2.

2.1 VUV lamp as reagent ion source in CIMS

Iodide reagent ions in the CIMS were generated using a VUV lamp mounted in front of the IMR. The VUV lamp (10.6 eV photon energy, PKR 106, Heraeus, Germany) was powered with a current of 2 mA at 1500 V DC. An electronic pre-filter was used to reduce noise from the switching power supply (Fig. S1).

Two major changes were implemented in our setup in contrast to the VUV lamp assembly described by Ji *et al.*[59] First, an acceleration voltage of 5 V was used for the ions to guide them into the IMR, which doubled the reagent ion yield. Second, the reagent ion flow was directed towards the VUV lamp before leaving the photo-ionization region. This has the advantage of maximizing the irradiance of the reagent gas shortly before the ions enter the IMR and requires less accurate alignment of the VUV lamp in its stainless-steel tube. A detailed overview of the differences between the VUV lamp and ^{210}Po ion sources with regard to the characteristics of Iodide-CIMS spectra can be found in Ji *et al.*[59]

2.2 Calibration of chlorine-containing species

Relative humidity dependent calibrations of Cl_2, $ClNO_2$, $ClONO_2$, HOCl and N_2O_5 were conducted post-campaign. In addition, we examined the effect of adding O_3 to flows of $ClNO_2$ and HOCl to assess potential secondary ion chemistry including the formation of $IClONO_2^-$ and IHO_2Cl^- (presented in SI). A summary of calibration curves for $ClNO_2$, $ClONO_2$, Cl_2 and HOCl can be found in Fig. S3. Higher mixing ratios than found in the atmosphere were used to enable simultaneous detection with less sensitive but absolute methods *e.g.*, CRDS and FT-IR with dynamic dilution for the CIMS.

An expression for the humidity-dependence of the calibration signal (for constant trace-gas mixing ratio) is given by polynomial fits (Fig. S4) that cover the full ambient humidity, *i.e.*, $IH_2O^-/(I^- + IH_2O^-)$ range so that no extrapolation beyond these humidities was necessary. Uncertainties associated with the humidity-dependent calibrations and the detection limits

Table 1 Calibrated chlorine species with detection limit (LoD, as 3 × σ for an averaging period of 5 min) as found for noise in the laboratory (LoD lab) and in the field (LoD campaign), calibration method and associated uncertainty. Thermal decomposition and non-destructive cavity ring-down spectroscopy (TD-CRDS and CRDS) were used as reference instruments[a]

Species	I^--cluster/m/z	LoD lab/pptv	LoD campaign/pptv	Calibration method	Uncertainty/%
Cl_2	196.843	0.05	0.03	Direct (Cl_2 gas), CRDS	7[a]
HOCl	178.877	3.50	2.21	Indirect (HOCl-to-Cl_2 conversion)	8[b]
$ClNO_2$	207.867	0.19	0.10	Indirect (N_2O_5-to-$ClNO_2$ conversion), TD-CRDS	28[c]
$ClONO_2$	223.862	0.20	0.36	Direct (synthesis), FT-IR	12[d]
N_2O_5	234.886	0.12	0.03	Direct (synthesis), TD-CRDS	28[e]

[a] Uncertainties calculated *via* error-propagation considering *e.g.* calibration methods and the linear regression of the calibration curves (Fig. S3 and S4): [a]<7% (mainly uncertainty in Cl_2 cross-sections[56] and humidity correction). [b] ∼8% (measurement uncertainty in Cl_2 and humidity correction, assumes 100% conversion of HOCl to Cl_2.) [c] 28% (same as N_2O_5, assumes 100% conversion of N_2O_5 to $ClNO_2$). [d]12% (uncertainty in $ClONO_2$ IR-cross-sections[57] and humidity correction). [e]28% (uncertainty in NO_2 cross-sections and conversion of N_2O_5 to NO_2.[58] Uncertainty in dilution factor is based on a flow controller uncertainty of 0.6%. The uncertainty associated with the humidity dependence function is: HOCl: 3.7%, Cl_2: 5.3%, $ClNO_2$: 0.9%, $ClONO_2$: 6.1% and N_2O_5: 1.5%.

during the campaign and laboratory calibration are presented in Table 1.

2.2.1 Cl_2. A canister of Cl_2 in N_2 was prepared by diluting a 5%, commercially obtained mixture in N_2 to 6 ppm. A small flow from the canister was dynamically diluted prior to simultaneous detection with the CIMS and a cavity ring-down spectrometer[60] operating at 405 nm where Cl_2 has a well-known absorption cross-section.

2.2.2 N_2O_5. N_2O_5 was synthesized by flowing a mixture of NO and a large excess of O_3 into a 2 L glass reaction chamber where they reacted for ≈1 min.[61] The exhaust, containing N_2O_5 and O_3, passed through a glass tube at −78 °C (dry ice/acetone bath) to trap the N_2O_5 as pure crystals. For calibration of the CIMS, the head-space above the N_2O_5 crystals (at −60 °C) was flushed with N_2 carrier gas to generate a dilute N_2O_5 gas mixture,[58] which was simultaneously sampled by the CIMS and a thermal dissociation cavity ring down spectrometer designed for measurement of N_2O_5 and NO_3.

2.2.3 $ClNO_2$. The CIMS was calibrated for $ClNO_2$ by converting a known amount of N_2O_5 (from a prior N_2O_5 calibration) to $ClNO_2$. This was achieved flowing the N_2O_5 flow through a glass reactor internally coated with dried NaCl at room temperature. The $ClNO_2$ generated this way was assumed to be equivalent in concentration to the N_2O_5 lost as shown in laboratory experiments investigating the heterogeneous uptake of N_2O_5 to dry sea-salt.[54,62]

2.2.4 $ClONO_2$. $ClONO_2$ was synthesized by allowing Cl_2O to react with N_2O_5 for several hours at −10 °C. Cl_2O was prepared by passing a flow of gaseous Cl_2 through a sample of HgO dispersed in glass-beads at −10 °C.[57] The $ClONO_2$ sample was used to generate a diluted sample in N_2 in a glass-bulb. The contents of the bulb were analyzed using a FTIR-spectrometer (Bruker Vector 22, Bruker Corporation, USA) at 0.5 cm^{-1} resolution. The absorption features of $ClONO_2$ were consistent with those reported by Davidson *et al.*,[57] whose integrated band-strengths were used to quantify the $ClONO_2$ mixing ratio in the glass-bulb to be 200 ppmv. The CIMS was calibrated by sampling $ClONO_2$ from the storage bulb with known dilutions in N_2.

2.2.5 HOCl. HOCl was generated by bubbling 30 sccm N_2 through a NaOCl solution (11–14% active chlorine) and diluting this flow with 10 sLpm N_2 (Fig. S5) The gaseous mixture was then directed through a glass U-tube at −40 °C to condense moisture prior to sampling by the CIMS. To quantify the HOCl content, the HOCl flow was alternatively directed through a U-tube containing a frozen, diluted HCl solution at −40 °C, which converts HOCl to Cl_2. The amount of HOCl was determined by measuring the depletion of HOCl and the generation of Cl_2 (for which the CIMS was already calibrated) according to Lawler *et al.*[11] It was crucial to remove moisture before directing the HOCl gas to the iced HCl surface, to prevent Cl_2 depletion due to uptake on moist surfaces. The uncertainty associated with the HOCl calibration does not consider the potential non-stoichiometric conversion to Cl_2 in the second U-tube, which, given the high vapor pressure and non-polarity of Cl_2 is expected to be negligible.

2.3 BISTUM24 field campaign: measurement site and instrumentation

The BISTUM24 field campaign took place from June 6 to 22, 2024 in Spielberg, central Germany (50°19′N, 9°15′E, Fig. S6). The rural measurement site, which is located 391 m above mean sea level on top of a hill in a treeless clearing, was selected because air masses encountered at the site originate mainly from rural regions and are rarely influenced by urban pollution despite the proximity to the Frankfurt metropolitan area (∼45 km). With a distance of ∼400 km to the next coastline, the North and Baltic Seas, the site may be described as continental with no direct marine influence (Fig. 2a and b).

The instruments used in this study sampled from inlets at a height of 6 m (Fig. S7) and were housed in the "Mobile Laboratory".[63] These included the Iodide-ToF-CIMS and an Aerosol Mass Spectrometer (AMS, Aerodyne Research Inc., USA), as well as an O_3 monitor (TB205, Monitor 205 Dual Beam Ozone Monitor, 2B Technologies, Inc., USA) and a pyranometer (CMP3 Pyranometer Sensor, Campbell Scientific Inc., UK). The surface area and volume of aerosol particles were calculated from

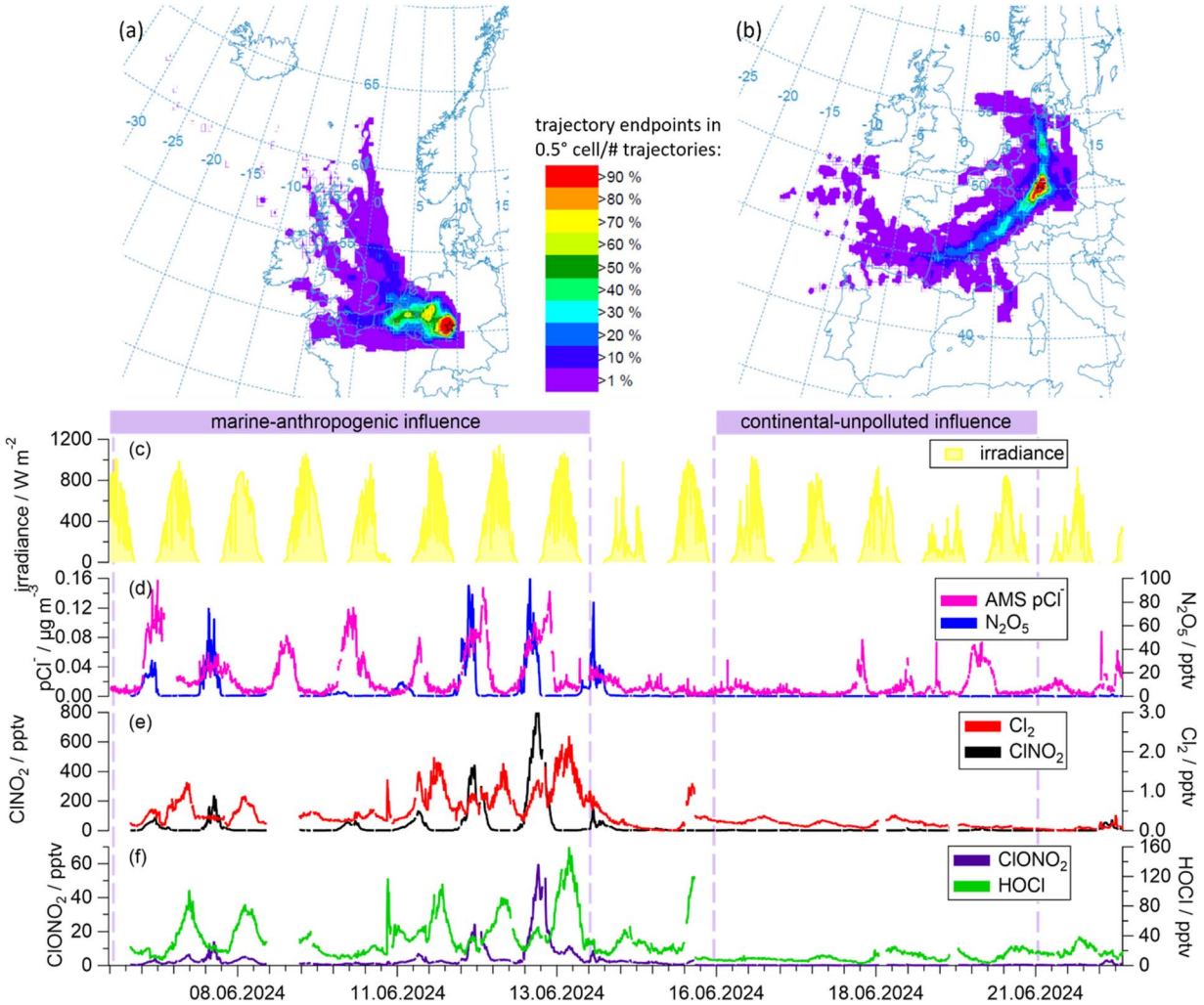

Fig. 2 Upper panels: 48 h-backward trajectories indicate that air masses in the period June 6 to 14, 2024 passed over marine and industrialised source regions (a). Between June 16 to 21, 2024 the air passed over rural, continental regions (b). Lower panel: time series of irradiance (c), chlorine trace gas precursor compounds particulate chloride (pCl^-) and N_2O_5, (d) and gaseous chlorine-containing species (e and f) measured during BISTUM24. The period between the 1st and 2nd dotted lines is designated "marine-anthropogenic", the period between the 3rd and 4th dotted lines is "continental-unpolluted".

a merged size distribution from different particle sizers (Fast Mobility Particle Sizer Model 3091, TSI, Inc., USA and Optical Particle Counter Model 1.109, Grimm Aerosoltechnik GmbH, Germany).[64] Local meteorological information was provided by a meteorological station (WXT520, Vaisala Oyj, Finland).

The CIMS was connected to the inlet *via* 6 m of PTFE tubing for which the residence time was ~1 s (corresponding to a total flow of 32 L min^{-1}). The CIMS sub-sampled 2 L min^{-1} from this flow. The inlet line also included a PTFE-particle filter, which was changed after every 20 000 liters of sampled air. While heterogeneous conversion of chloride to chlorine trace gases on filters or inlet lines can be an issue in coastal regions with high sea-salt loadings,[11,65] this is not expected to occur at the present location where chloride is not associated with sea-salt. The non-observation of $ClNO_2$ formation despite the presence of high concentration of N_2O_5 and the use of "aged" inlet lines supports this assumption. Zero measurements were performed every 8 h for 20 min during the campaign using humidified N_2. The CIMS data were zero-corrected, and the signal at each mass analyzed was normalized to the sum of the most abundant reagent ions, I^- and IH_2O^-. Calibration factors were applied, determined as described in Section. 2.2.

3 Chlorine-containing compounds and air mass origin

Fig. 2 provides a time series of the chlorine-containing trace gases $ClNO_2$, $ClONO_2$, HOCl, Cl_2 and N_2O_5, measured by the CIMS, as well as particulate chloride (pCl^-) as measured by the AMS. Although the AMS does not efficiently detect pCl^- from sea salt, it can detect pCl^- from, *e.g.*, ammonium chloride. For this reason, pCl^- does not necessarily represent the total amount of particulate chloride present in the particle phase. Information on airmass origin was gained using HySplit[66,67]

with which 48-h backward trajectories ending 30 m above ground level at the measurement site were calculated.

In the first phase (June 6 to 14), back-trajectories showed that the air passed over the English Channel and industrialized regions in Belgium and the Netherlands, as well as the German Ruhr metropolitan area before reaching the measurement site. The transport times were 12 to 36 h for UK and Benelux and 4 to 6 h for the Ruhr region, respectively. During transport, trajectories rarely exceeded altitudes of 500 m above mean sea level, indicating that the air was transported within the boundary layer. We refer to the air masses in this period as having a "marine-anthropogenic" influence as evidenced by the enhanced levels of pCl^- and N_2O_5 (Fig. 2d).

In contrast, backward trajectories for the period June 16 to 21 indicate that the air sampled during this period travelled at altitudes > 1000 m above mean sea level for several days before descending close to the measurement site. The vast majority of these trajectories passed over the relatively sparsely populated, non-industrialized center of France and rural south-west Germany (Fig. 2b and S8b). We designate these air masses as "continental-unpolluted". In these air masses, N_2O_5 was generally below the detection limit and concentrations of pCl^- were much lower than those of the other air masses.

As expected, the mixing ratios of Cl_2 and $ClNO_2$ were largest during the "marine-anthropogenic" period, with $ClNO_2$ exceeding 70 pptv every night and Cl_2 exceeding 0.5 pptv every day (Fig. 2e). HOCl and $ClONO_2$ were less abundant than $ClNO_2$, with mixing ratios of up to 60 pptv (Fig. 2f). During this period, mean mixing ratios of 56.2 pptv $ClNO_2$, 0.64 pptv Cl_2, 41.3 pptv HOCl and 4.8 pptv $ClONO_2$ were observed, whereas during the "continental-unpolluted" period, 2.25 pptv $ClNO_2$, 0.17 pptv Cl_2 and 11.1 pptv HOCl were measured and $ClONO_2$ levels were below the detection limit.

Worldwide, the mixing ratios of inorganic chlorine species vary considerably depending on the air masses sampled and the geographical location. Our $ClNO_2$ mixing ratios are consistent with those observed at continental sites with similar (indirect) marine-influenced air masses, which show peak $ClNO_2$ concentrations of 300–700 pptv.[13,14] These mixing ratios are higher than those measured in maritime air,[22,48] which results from a longer residence time over landmasses with a greater anthropogenic influence, which is crucial for the formation of $ClNO_2$ (see Section. 1). Consequently, for highly polluted sites like in Hong Kong or Los Angeles up to 3.5 ppbv of $ClNO_2$ have been reported.[68,69]

During both periods of the BISTUM24 campaign, the Cl_2 levels were generally low compared to those reported in other studies, especially those influenced by highly polluted urban regions.[48,70] Cl_2 mixing ratios in the marine boundary layer vary from ~2 to ~500 pptv[11,48,69,71,72] and are enhanced compared to rural continental sites ranging from ~2 to ~33 pptv,[22,73] depend heavily on the agricultural land use in region. There are no previous reports of $ClONO_2$ measurements in lower troposphere with which to compare our data.

Results from our HOCl measurements are broadly consistent with the 2–120 pptv HOCl range reported for continental and marine air masses.[11,48] The large variability is related to air mass history, even when only marine regions are considered.

Fig. 2 reveals substantial differences in the diel profiles of the trace gases measured. N_2O_5 and $ClNO_2$ were observed predominantly at nighttime whereas HOCl and Cl_2 were observed predominantly during the day. The absence of N_2O_5 during the day is expected ((R2), Section 1) and, as N_2O_5 is the precursor of $ClNO_2$, the nighttime dominance of the latter is also consistent with present knowledge of its production and loss terms (Section 1). pCl^- has a less clear day–night variation which is related to the presence of multiphase equilibria, whereby chloride is present as a dissolved ion in the particle phase or degassed from aerosols as HCl. For the mixing ratios of $ClONO_2$, the two strongest features were observed after midnight on the nights of 13th and 14th June with strong covariance with $ClNO_2$. This was unexpected, as $ClONO_2$ is believed to be formed exclusively in the reaction of ClO with NO_2, with the ClO-radical being present at significant levels only during the daytime when photochemically generated Cl atoms react with O_3.

While many studies have reported $ClNO_2$ and Cl_2 in coastal regions[39,48,54,74] or in highly polluted regions where non-marine chloride sources exist,[12,32,33,75] only few[10,13,22] have identified reactive chlorine trace-gases in air masses that may be described both as non-marine (*i.e.*, several hundred km from coastal regions) and also not impacted by local pollution. Of these, only Phillips *et al.*[13] investigated chlorine chemistry in mainland Europe. They argued that, as coarse mode sea-salt particles are not efficiently transported hundreds of km, the source of particle chloride was HCl that was released from coarse-mode sea-salt particles close to coastal regions (by, *e.g.*, acid displacement) and subsequently transported as gas phase HCl or particulate ammonium chloride. As Phillips *et al.*[13] did not measure other chlorine-containing trace-gases apart from $ClNO_2$, they did not consider the potential role of HOCl, Cl_2 or $ClONO_2$ in, *e.g.*, the production rate of Cl atoms or OH radicals.

4 The diel cycle of Cl_2, HOCl, $ClNO_2$ and $ClONO_2$

Fig. 3 displays the mean, fractional contribution of each individual chlorine-containing trace gas to the total inorganic chloride mixing ratios during BISTUM24. For the "marine-anthropogenic" influenced phase (a), $ClNO_2$ is dominant during the night (max. ~70%), with HOCl being dominant during the day (max. ~90%) and $ClONO_2$ and Cl_2 representing only a few percent of overall chlorine-containing species throughout the diel cycle. During the "continental-unpolluted" phase (b), HOCl is the dominant chlorine-containing trace gas both day and night, accounting for > 60% during the night and >80% during the day. Both $ClONO_2$ and Cl_2 are minor contributors with ~1% each, while the nocturnal $ClNO_2$ contribution is relatively low due to N_2O_5-poor conditions (~30%). The diel profile of $ClNO_2$ is understood in terms of its generation through multiphase chemistry involving N_2O_5 during the night, followed by its daytime photolysis to release Cl atoms that (*via* reactions of HO_2

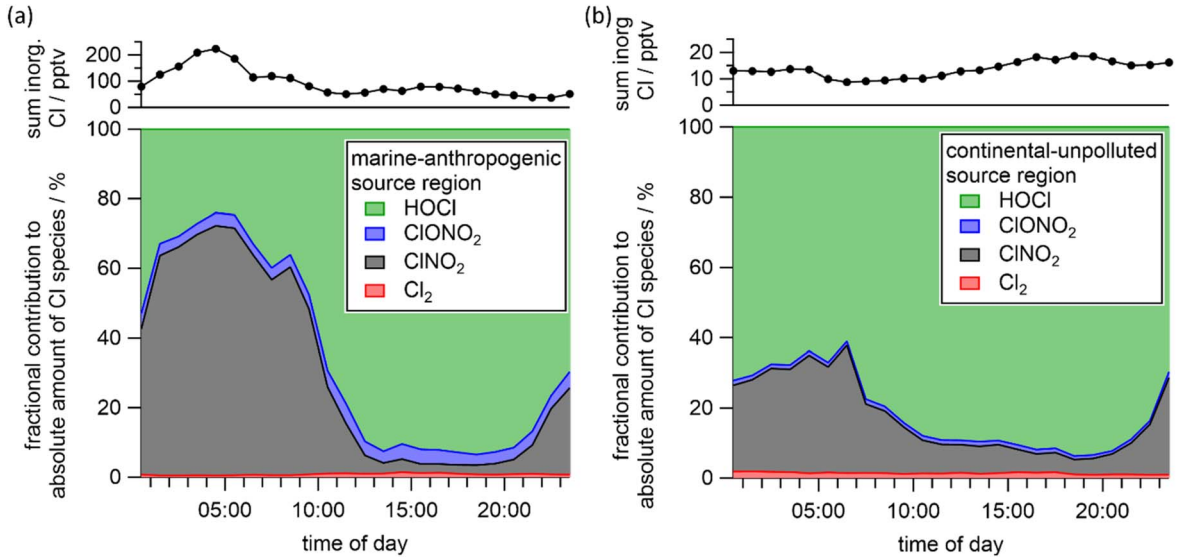

Fig. 3 Diel cycle of the fractional contribution of inorganic chlorine species to the summed mixing ratio. The data are separated into air masses designated "marine-anthropogenic" (a) and "continental-unpolluted" (b). $ClONO_2$ in (b) is at the detection limit.

and ClO) lead to daytime HOCl. The significant nighttime contribution of HOCl is likely related to incomplete loss from the previous day rather than nocturnal formation, for which a non-radical mechanism is unknown. The heterogenous loss rate coefficient (k_{het}) for HOCl with respect to uptake on aerosol particles was calculated with eqn (1):

$$k_{het} = 0.25\gamma A c_{HOCl} \quad (1)$$

with the mean molecular velocity $c_{HOCl} = 34\,700$ cm s^{-1}, derived from the molecular weight of the gas species for 298 K, the mean aerosol particle surface during the campaign $A = 130$ μm^2 cm^{-3}, which is representative also for nighttime (Fig. S10), and the uptake coefficient $\gamma < 2 \times 10^{-4}$ that is available for particles with pH = 1.[34]

The calculated lifetime of HOCl due to uptake on acidic particles ($k_{het}^{-1} \approx 5$ days) is much longer than the lifetime with respect to photolysis (~1 h, Table 2). Hence, the observed nighttime HOCl was most likely generated photochemically the previous day.

Table 2 Photolysis rate J and lifetime of photolabile species at noon from.[76]

Species	J s^{-1}	Lifetime min
$O_3(^1D)$	3.52×10^{-5}	473
$ClNO_2$	4.97×10^{-4}	33.5
$ClONO_2$	4.97×10^{-5}	335
Cl_2	2.43×10^{-3}	6.9
HOCl	2.86×10^{-4}	58.3
NO_3	2.37×10^{-2}	0.7
N_2O_5	4.78×10^{-5}	349[a]

[a] Thermolabile N_2O_5 forms NO_3 during daytime in an equilibrium. Fast photolysis of NO_3 significantly decreases the N_2O_5-lifetime.

4.1 $ClNO_2$

In the following, we investigate the formation and loss of $ClNO_2$ through the diel cycle during the "marine-anthropogenic" period and highlight the influence of air mass history and vertical mixing on the $ClNO_2$ abundance during two individual night–day transitions.

In Fig. 4 we present the median, diel cycles of the mixing ratios of $ClNO_2$, $ClONO_2$ and N_2O_5 over the entire "marine-anthropogenic" time period. The diel cycle is divided into three phases which represent (I) nighttime, when N_2O_5 is present, (II) the period just after sunrise when N_2O_5 is rapidly depleted and the mixing ratios of $ClNO_2$ and $ClONO_2$ are either constant or

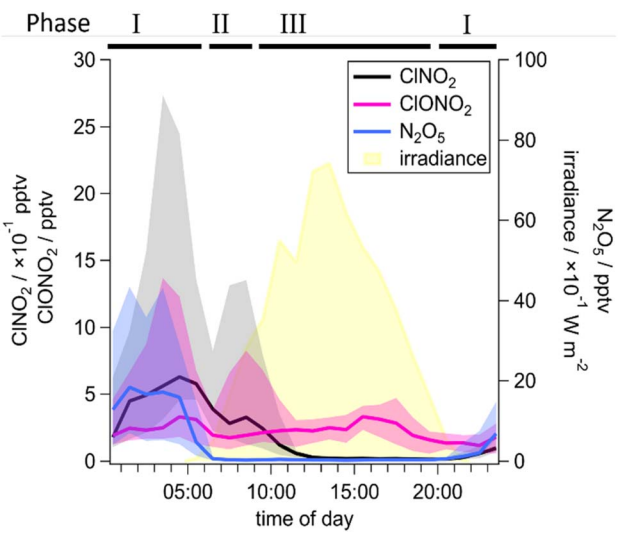

Fig. 4 Diel cycle of $ClNO_2$ (black) and $ClONO_2$ (pink), N_2O_5 (blue) and irradiance (yellow) during the "marine-anthropogenic" period of the BISTUM24 campaign in local time. Lines represent the median; the interquartile ranges are given as shaded area.

increasing, and phase III when irradiance is stronger and $ClNO_2$ mixing ratios decrease monotonically to zero.

The formation of $ClNO_2$ depends on the presence of N_2O_5 and pCl^- (R1) and thus we expect net-production only when N_2O_5 and pCl-are present. The data in phase I and II from June 10 and 12, 2024 show that this is not always reflected in the $ClNO_2$ mixing ratios which remain constant or sometimes even increase during the early morning when N_2O_5 is absent, although the photolytic loss of $ClNO_2$ increases with intensifying irradiance. Note that, subsequent to a post-dawn peak, the $ClNO_2$ mixing ratios decrease with a decay constant of 5×10^{-4} s^{-1} in accord with J_{ClNO_2} (Table 2).

At the beginning of the night from June 12, from 21 : 00 to 01 : 30 (Fig. 5a), an approximately linear increase in $ClNO_2$ of (19 ± 1) pptv h^{-1} was observed. The $ClNO_2$ production rate can be calculated from k_{het}, the N_2O_5 mixing ratio and the fraction α of N_2O_5 that forms $ClNO_2$:

$$P(ClNO_2) = [N_2O_5]\alpha k_{het} \quad (2)$$

where k_{het}, was calculated from the uptake coefficient for N_2O_5 to an aqueous surface $\gamma = 0.02$,[34] the aerosol surface area in this period $A = 104$ μm^2 cm^{-3} and the mean molecular velocity of N_2O_5 $c_{N_2O_5} = 27\,800$ cm s^{-1}. Considering a mean $[N_2O_5] = 18$ pptv, and $\alpha = 0.8$ given for a 0.22 M chloride in particles,[62] a $ClNO_2$ production rate of 7.7 pptv h^{-1} is obtained. Given the factor 3 uncertainty in γ[34,77] and the AMS uncertainty in pCl^- and thus,[78] the calculated $P(ClNO_2)$ is consistent with the observed, net $ClNO_2$ formation rates.

After 01 : 30 the $ClNO_2$-to-N_2O_5 ratio switches from ~2 to ~6, and the high $ClNO_2$ levels in the next 4 h cannot be explained by local production from N_2O_5. This trend continues in phase II in Fig. 5a, where an increase in pCl^- (up to 1 M Cl^-) was accompanied by an increase in $ClNO_2$ levels although N_2O_5 levels were close to zero. A similar picture emerges from the data in Fig. 5b, in which post-dawn peaks in $ClNO_2$ (~55 pptv between 05 : 00 and 06 : 00 and ~69 pptv between 08 : 20 and 09 : 20) are observed despite the production term (in the absence of N_2O_5) being zero. In both cases, the *in situ* production of $ClNO_2$ from N_2O_5 reaction with pCl^- can be ruled out and the increase in $ClNO_2$ after dawn is attributed to the sampling of air masses in which N_2O_5 had been previously converted to $ClNO_2$. This simply reflects the fact that $ClNO_2$ is substantially longer-lived during the day than N_2O_5 as J_{ClNO_2} is much lower than J_{NO_3} (which controls the N_2O_5 lifetime due to its equilibrium with N_2O_5).

The phase II, post-dawn peaks in $ClNO_2$ were found to be enhanced for those days when backward trajectories showed subsiding air masses 1–3 h before the air reached the measurement site (see interquartile range in Fig. 4). The air from higher altitudes entrains O_3-rich residual layer air into the nocturnal boundary layer,[79] which results in enhanced formation of N_2O_5 and thus of $ClNO_2$. Additionally, at dawn when the nocturnal boundary layer dissipates through radiative heating and convective mixing of air from the residual layer, O_3-rich air may be transported to the surface. The daily development and breakdown of the nocturnal boundary layer can also cause variability in $ClNO_2$ levels due to vertical mixing.

4.2 $ClONO_2$

While $ClNO_2$, has been measured in the lowermost troposphere on many occasions,[10,12–14] the detection of $ClONO_2$ during BISTUM24 was unexpected. Previous studies have demonstrated the potential of using CIMS methods with SF_6^- and I^- to measure $ClONO_2$ as $FClNO_3^-$ and $IClNO_3^-$,[15,75] and airborne SF_6^--CIMS measurements have quantified $ClONO_2$ in the upper troposphere where its presence (at levels up to 10 pptv) was explained by the entrainment of stratospheric air.[15]

Our study presents the first quantitative ambient ground-level $ClONO_2$ measurements using Iodide-CIMS. As already mentioned, the accepted mechanism for formation of atmospheric $ClONO_2$ is (R8), which requires the presence of ClO and NO_2. ClO is a radical that is formed as a result of photochemical processes and expected to be present predominantly during daytime; we therefore expect reaction (R8) to be responsible for the net increase in $ClONO_2$ observed during the day (Phase III in

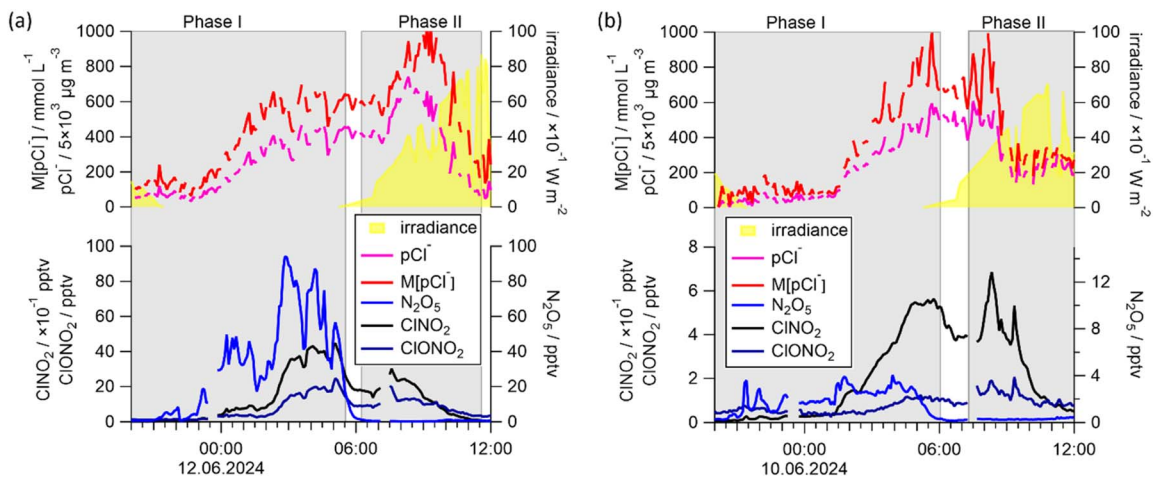

Fig. 5 Mixing ratios of $ClNO_2$ (black), $ClONO_2$ (dark blue) and pCl^- (as mass (pink) and molar (red) concentration) through the diel cycle on June 10 (a) and 12 (b), 2025.

Fig. 5). However, following this line of reasoning $ClONO_2$ is not expected to be formed in significant rates during the night, which we nonetheless observe (Phase I in Fig. 5). In the following, we first calculate the $ClONO_2$ lifetime and then estimate the production rate that would be required to maintain the observed levels. The photolysis frequency of $ClONO_2$ is 4.97×10^{-5} s^{-1}, resulting in a lifetime of ~5–6 h with respect to this loss process ((R13), Table 2). The heterogeneous loss frequency of $ClONO_2$ was calculated from eqn (1) with the uptake coefficient on aqueous particles $\gamma = 0.027$ and $c_{ClONO_2} = 25\,590$ cm s^{-1}.[34] Using a campaign mean particle surface area density A of 130 μm^2 cm^{-3} results in a loss rate constant of $k_{het} = 2.25 \times 10^{-4}$ s^{-1}, or a lifetime of ~75 min. Given this short lifetime with respect to heterogeneous uptake, $ClONO_2$ cannot survive from the previous day and, in the absence of sources, its mixing ratios should tend to zero in the first hours during the night. In order to explain the observed mean $ClONO_2$ mixing ratio of 4.3 pptv at 05 : 00 during the night, we require a nocturnal production rate of $\sim 2.4 \times 10^4$ molecules cm^{-3} s^{-1}, which can be equated to $P(ClONO_2) = k_{NO_2+ClO} \times [ClO] \times [NO_2]$. Assuming an NO_2 mixing ratio of 1–2 ppbv during the "marine-anthropogenic" period as measured at a similar site with similar prevailing wind direction[80] and that the sole source of $ClONO_2$ is the reaction between ClO and NO_2 (with a rate coefficient, k_{NO_2+ClO}, at 298 K and 1 bar of 2.4×10^{-12} cm^3 $molecule^{-1}$ s^{-1}, IUPAC) we calculate that the ClO concentration necessary to maintain this level of $ClONO_2$ is $[ClO] = (2–4) \times 10^5$ molecules cm^{-3}, where the spread in values results from the range of NO_2 mixing ratios assumed for the calculation.

A well-known source of gas phase ClO is the reaction between Cl atoms and O_3 (R6). Thus, the presence of nighttime $ClONO_2$ would require a reaction that generates either Cl atoms or ClO directly, both in the absence of sunlight. The conversion of Cl to ClO is directly influenced by O_3 levels and competing Cl reactions with, *e.g.*, hydrocarbons and NO_X trace gases. The loss rate constant of Cl through its reaction with O_3 is given as $k_{Cl+O_3} \times [O_3] = 11.8$ s^{-1} (calculated from the mean average O_3 concentration (40 ppbv) and the rate coefficient $k_{Cl+O_3} = 1.2 \times 10^{-11}$ cm^3 $molecule^{-1}$ s^{-1})[34].

The first-order loss rate constant of Cl atoms reacting with the most abundant alkanes can be calculated from $k_{Cl+CH_4} \times [CH_4] + k_{Cl+C_2H_6} \times [C_2H_6] + k_{Cl+C_3H_8} \times [C_3H_8]$. As concentrations of these hydrocarbons were not measured during the campaign, we use reference mixing ratios of 1.9 ppm CH_4, 0.8 ppbv C_2H_6, and 0.3 ppbv C_3H_8 that are typical for rural continental conditions and the corresponding rate coefficients with Cl.[34,81] The calculated total loss rate constant for reaction with these hydrocarbons is ~6.8 s^{-1}, with the largest single contributions from methane (4.6 s^{-1}, *i.e.*, ~25% of Cl). We acknowledge that loss of Cl atoms due to terpenoids can be significant, however, their concentration is highly variable (even in rural continental regions) and their contribution is highly uncertain (considering 1 ppbv terpenoids with $k_{Cl+isoprene} = 4.6 \times 10^{-10}$ molecules cm^{-3} s^{-1} would result in a loss rate to terpenoids of ~11.2 s^{-1},[82] *i.e.*, the same as the loss rate to O_3 adding a uncertainty factor of 2 to the calculation). Cl atoms react with NO_2 with a rate coefficient of 6.7×10^{-12} cm^3 $molecule^{-1}$ s^{-1} campaign conditions.[83] Assuming (as above) that NO_2 mixing ratios were between 1 and 2 ppbv at night results in a Cl atom loss rate constant of ~0.3 s^{-1}.

Taking the formation rate of ClO from Cl (11.8 s^{-1}) and the loss rates of Cl through other pathways (6.8 s^{-1} and 0.3 s^{-1}), we can conclude that approximately 60% of the Cl atoms generated react to form ClO. We can estimate the production rate of ClO by assuming that its concentration is in steady state with respect to its gas phase formation and loss processes at night. In the absence of NO, the dominant loss process for ClO at night is its reaction with NO_2, with a loss rate of 2.4×10^4 molecules cm^{-3} s^{-1}. Using the 60% ClO yield from Cl, this in turn can be converted into a Cl atom production rate $P(Cl) = k_{NO_2+ClO} \times [ClO] \times [NO_2]/0.6 = (2.0–3.9) \times 10^4$ atoms cm^{-3} s^{-1}.

We now examine potential reactions that, at nighttime, could lead to Cl atom production rates of this magnitude. The dominant radical at nighttime is often considered to be NO_3, which initiates the oxidation of many biogenic hydrocarbons. However, reactions of NO_3 radicals with sufficiently abundant (non-radical) chlorine species to generate ClO or Cl atoms are either unknown or expected to be too slow to contribute significantly. For example, the rate coefficient for the reaction between NO_3 and HCl (R14) is $< 5 \times 10^{-17}$ cm^3 $molecule^{-1}$ s^{-1},[34] which would result in a maximal Cl atom production rate of 1.2×10^2 atoms cm^{-3} s^{-1}, if we assume typical mixing ratios of 100 pptv HCl[84,85] and 10 to 40 pptv NO_3,[80] which is a factor ~350 lower than that required.

$$HCl + NO_3 \rightarrow Cl + HNO_3 \quad (R14)$$

As the reaction between NO_3 and HCl cannot explain the nighttime production of Cl atoms, we consider the potential role of OH radicals, which react much more rapidly with HCl ((R15), $k_{OH+HCl} = 7.8 \times 10^{-13}$ cm^3 $molecule^{-1}$ s^{-1})[34].

$$HCl + OH \rightarrow Cl + H_2O \quad (R15)$$

OH radicals are present at night owing to their formation in the ozonolysis of unsaturated hydrocarbons,[86,87] and their abundance has been the subject of much research, with concentrations found to be varying between 9.1×10^4 and 7×10^6 molecules cm^{-3} at night time.[88–91] Due to the absence of OH measurements during BISTUM24, we assume a nighttime concentration of 1×10^5 molecules cm^{-3} that was determined in a similar agricultural rural environment.[88] For the HCl mixing ratio, we assume a value of 100 pptv HCl (as measured over the continent[85]) and calculate a Cl production rate of 1.9×10^2 atoms cm^{-3} s^{-1}, which is a factor 100–200 smaller than the value of $(2.0–3.9) \times 10^4$ atoms cm^{-3} s^{-1} derived above.

The nocturnal ozonolysis of unsaturated hydrocarbons also leads to the formation of Crigee-intermediates.[87,92] Studies of the reaction of HCl with Crigee-intermediates appears however not to form Cl or ClO but R_1R_2OOCl compounds, where R_1 and R_2 are organic groups.[93]

In addition, we also consider the direct formation of ClO through the reaction of OH with HOCl (R16):

$$HOCl + OH \rightarrow ClO + H_2O \quad (R16)$$

for which the rate coefficient at 298 K is $k_{OH+HOCl} = 5.0 \times 10^{-13}$ cm^3 molecule^{-1} s^{-1}.[34] Assuming again an OH concentration of 1.0×10^5 molecules cm^{-3} during night[88] and nocturnal campaign mean mixing ratio of 50 pptv for HOCl we derive a ClO production rate of 1.2×10^3 ClO cm^{-3} s^{-1} which is a factor ten larger than the rate of formation of Cl from OH + HCl but falls well short of the value required to explain the observations of nighttime $ClONO_2$.

We thus conclude that the presence of $ClONO_2$ at nighttime, despite its rapid heterogeneous loss to particles, cannot be explained by the OH-induced conversion of HCl and HOCl to Cl and ClO, even within the major uncertainties related to the estimations of the HCl and OH levels. We note however, that nighttime Cl levels of 2.0×10^4 atoms cm^{-3} have been reported in the urban UK,[91] although the authors were not able to name a Cl source. Such levels of Cl result in a ClO production rate of 2.4×10^5 molecules cm^{-3} s^{-1} which is a factor 10 larger than at required to explain our observations.

At this point, we examine the possibility that $ClONO_2$ is actually significantly longer lived at night than so far calculated based on an uptake coefficient of $\gamma = 0.027$,[34] which is the result of laboratory experiments performed on inorganic aqueous solutions containing sulphate, halides *etc.* We now draw analogy to the heterogeneous uptake to aqueous particles of another di-acid anhydride, N_2O_5 for which γ from laboratory studies is also very similar (~0.02).[34] In contrast to $ClONO_2$, the tropospheric, multiphase chemistry of N_2O_5 has been the subject of many studies and the rate of uptake to "real" atmospheric particles that are internal mixtures of organics, sulphates, nitrates *etc.* is a strong function of composition, where the presence of organic has been observed to reduce γ significantly.[94] As the mechanism of uptake of N_2O_5 and $ClONO_2$ to aqueous particles is expected to be similar (both hydrolyze/ionize on/at the surface) it is very possible that γ and the rate of uptake of $ClONO_2$ is greatly reduced compared to the values calculated above, and that the source term required to generate the observed mixing ratios of $ClONO_2$ is actually lower. In the absence of laboratory studies investigating the dependence of $\gamma(ClONO_2)$ on *e.g.*, particle organic content, this remains speculative. In addition, while no appropriate mechanism is known to us, we cannot rule out alternative (potentially multiphase) routes to $ClONO_2$ formation at nighttime may be more important than the gas phase reaction between ClO and NO_2.

However, to illustrate the potential importance of nocturnal Cl production we calculate its effect on the methane lifetime. Based on the measurement of $ClONO_2$, we derived a nocturnal Cl production rate of (2.0–3.9) $\times 10^4$ atoms cm^{-3} s^{-1} (see above). We can combine this with the fact that ~25% of the Cl atoms formed will react with CH_4 (see above) to calculate a CH_4 lifetime of ~45 years with respect to nocturnal loss *via* reaction with Cl atoms. Given that the lifetime (*i.e.*, the inverse reaction rate) of the important climate gas methane is of the order of 10 years (predominantly through reaction with OH) this translates to a ~15% fractional contribution to CH_4 loss. We note that this calculation is based on the assumption that $ClONO_2$ is formed solely *via* gas phase reaction of ClO and NO_2. A heterogeneous process forming $ClONO_2$ that does not require the formation of Cl atoms would have no effect on hydrocarbon oxidation rates. A more rigorous assessment of the global impact of regional chlorine activation, for example regarding the methane lifetime, requires further related observations, inclusion of realistic chlorine activation scenarios and chlorine photochemistry in global models.

4.3 Formation and diel cycle of Cl_2 and HOCl

Median diel cycles of HOCl and Cl_2 are depicted in Fig. 6 and show maxima of 60–70 pptv HOCl and 0.8–1.0 pptv Cl_2 in the afternoon (Fig. 6), implying that both are largely of photochemical origin. Strong correlations of Cl_2 ($R^2 = 0.88$) and HOCl ($R^2 = 0.85$) with O_3 (Fig. S11) indicate a photochemical source.

Cl_2 is known to be formed in the reaction between gaseous chlorine species such as $ClNO_2$, $ClONO_2$ and HOCl with pCl^- in acidified aerosol, which may help to explain the timing of the peak Cl_2 mixing ratio in the afternoon (phase III) after maximum irradiance ((R4), (R9), (R10), and Oum *et al.*[30]). In addition to the daytime peak, a slight increase in Cl_2 levels was monitored between 04 : 00 to 07 : 00, *i.e.*, between phase I and II. This observation may also be linked to the entrainment of O_3/N_2O_5-rich air from the residual layer into the nocturnal boundary layer (Section. 4.1) in agreement with Xia *et al.*,[95] so that particle chloride can be converted into chlorine-containing gases such as Cl_2 and $ClNO_2$. Cl_2 is also formed in other multiphase processes involving chloride and the intermediary of NO_3^-, $O(^3P)$, Fe(III) and TiO_2.[47,96–99]

For HOCl, the recognized and only atmospherically relevant route to its generation in the gas phase is through the reaction between two radical species, ClO and HO_2 (R7) which takes place predominantly during the daytime when active photochemistry leads to high radical concentrations. The particle phase hydrolysis of $ClONO_2$ (R11) also leads to the formation of

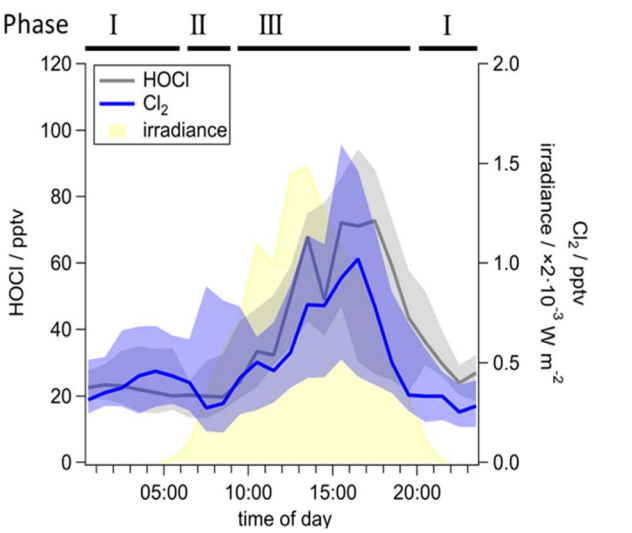

Fig. 6 Diel cycle of HOCl (grey) and Cl_2 (blue) mixing ratios and irradiance (yellow). Lines represent the median; the interquartile ranges are given as shaded area. The diel cycles only consider data from the "marine-anthropogenic" period of the BISTUM24 campaign.

HOCl, which can either degas from the particles or react with particle chloride to form Cl_2. As Cl_2 is weakly soluble, this will likely transfer to the gas phase where it is rapidly photolyzed (Table 2) to reform Cl atoms that, in turn, reform HCl and the HOCl precursor ClO. As HOCl is also photolabile, its gas phase mixing ratios are determined by chemical cycles that are strongly dependent on actinic flux and the availability of, *e.g.*, O_3.

5 Daytime Cl-atom production rates

While the OH radical is the primary driver of oxidation of the vast majority of atmospheric trace gases, the oxidation rates of certain trace gases can be augmented by the presence of Cl atoms. In this section, we examine Cl-atom production rates $P(Cl)$ from the photolysis of $ClNO_2$, $ClONO_2$, HOCl and Cl_2 ((R3), (R5), (R12) and (R13)) over the diel cycle:

$$P(Cl) = J_{ClNO_2}[ClNO_2] + J_{ClONO_2}[ClONO_2] + 2J_{Cl_2}[Cl_2] + J_{HOCl}[HOCl] \quad (3)$$

The photolysis frequencies J of $ClNO_2$, $ClONO_2$, HOCl and Cl_2 were derived for each trace gas through the diel cycle (data provided by the TUV calculator for cloudless conditions for the BISTUM24 location[76]), corrected for cloud-reduced irradiance, measured using a local on-site pyranometer. We recognize that clouds do not impact irradiance in the same way for all wavelengths; however, considering cloudiness provides a more accurate estimate of real photolysis rates.

The results of the calculations are summarized in Fig. 7 which shows that Cl production follows the actinic flux, reaching a maximum of $(1.0 \pm 0.47) \times 10^6$ atoms cm^{-3} s^{-1} in the period in which we sampled "marine-anthropogenic" air. The maximum for "continental-unpolluted" air is a factor ~6 lower $(1.6 \pm 0.7) \times 10^5$ atoms cm^{-3} s^{-1}. The daytime maximum Cl production rates are broadly consistent with summertime observations from Los Angeles[100] (6.2×10^5 atoms cm^{-3} s^{-1}), Houston[22] (4.7×10^5 atoms cm^{-3} s^{-1}), Beijing[75] (1.6×10^5 atoms cm^{-3} s^{-1}) and wintertime Manchester-UK[39] (3.0×10^5 atoms cm^{-3} s^{-1}). Note however, that the values for Houston considered only Cl_2 and $ClNO_2$ as Cl sources,[22] while additionally, for Los Angeles HCl + OH contributes significantly.[100] In the Beijing-study a minor role was attributed to HOCl and $ClONO_2$ (not quantified and considered in Le Breton *et al.*[75]) and $ClNO_2$ was considered to be the only Cl sources in marine urban Manchester.[39] The fact that Cl production rates were observed in polluted and marine influenced regions, as well as in rural continental areas (this work) indicates the role of Cl chemistry could be more widespread than currently assumed.

The fractional contribution of each chlorine-containing trace gas to Cl atom production rates is highlighted in Fig. 8. HOCl is the major contributor to Cl production from photolysis, accounting in the morning for 10% for "marine-anthropogenic" air masses and 49% for air masses from "continental-unpolluted" source regions. After ~12 : 00, the HOCl contribution is in both cases between 70% and 80% (see Fig. 8a and b).

Contrary to HOCl, the contribution of $ClNO_2$ to Cl production decreases from 85% at sunrise (07 : 00) to 3% after 13 : 00 if the air masses were transported from the "marine-anthropogenic" source region. The contribution of $ClNO_2$ in continental unpolluted air, meanwhile, is significantly lower, ranging from 6% to 33%. This observation emphasizes the importance of $ClNO_2$ as a nighttime reservoir species, particularly for air masses affected by polluted areas.

For air masses with marine-anthropogenic signature, Cl_2 contributes approximately 5% to Cl production rate in the morning hours, increasing to 20% from 13 : 00 on. Despite its much lower mixing ratios, after 11 : 00 the contribution of Cl_2 is larger than that of $ClNO_2$, which is related to the absorption cross section of Cl_2 which overlaps much more with the actinic flux (Fig. S12). The contribution of Cl_2 to Cl production rates

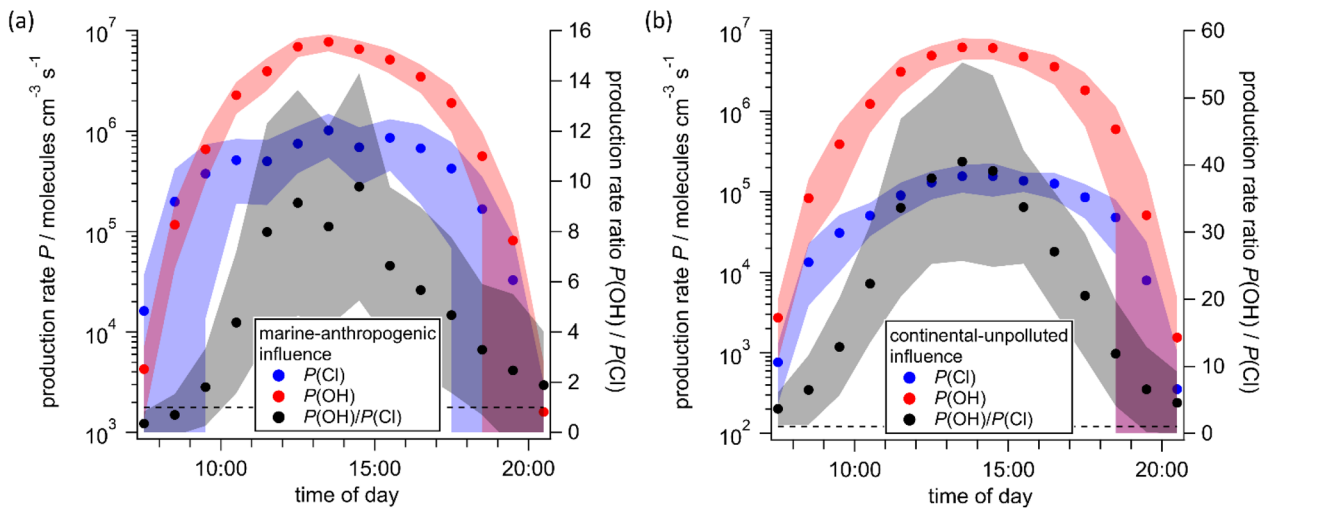

Fig. 7 Median production rates of Cl (P(Cl), blue) and OH (P(OH), red) as well as the ratio of the production rates (P(OH)/P(Cl), black) for the air masses with marine-anthropogenic (a) and with continental-unpolluted influence (b). The shaded areas represent interquartile ranges, while the dotted line indicates equal production of Cl and OH.

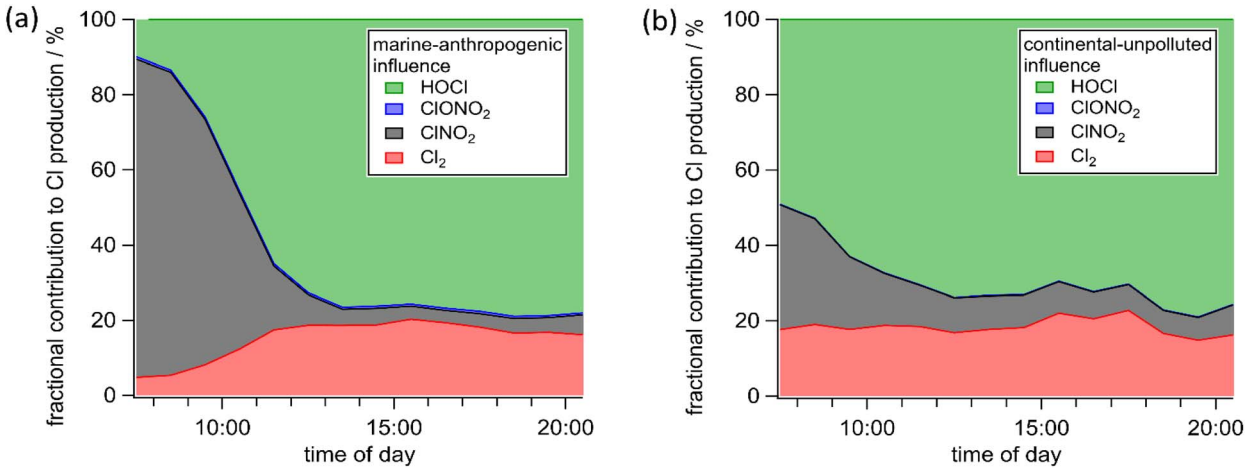

Fig. 8 Fractional contribution of various inorganic chlorine species to the diurnal total chlorine production rate for air masses with marine-anthropogenic (a) and with continental-unpolluted influence (b).

from continental unpolluted air remains around 20% throughout the day.

Low daytime concentrations of maximum 3.3 pptv, coupled with low absorption cross-sections at the wavelengths of the actinic flux, mean that $ClONO_2$ plays a minor role in Cl production. Fig. 8a indicates that $ClONO_2$ contributes only 0.5% to Cl production, independent of the time of day, which is consistent with conclusions of Le Breton *et al.*[75]

The impact of a summed, maximum daytime Cl production rate of $\sim 1 \times 10^6$ atoms cm^{-3} s^{-1} (at ~14 : 00 local time) can also be illustrated by estimating its impact on CH_4 oxidation. As discussed in Sect. 4.2, ~25% of the Cl atoms generated under these conditions will react with CH_4. The CH_4 loss due to Cl during one hour at noon is ~40 pptv. This can be compared to the CH_4 loss in the same period owing to reaction with OH, which is ~400 pptv, assuming OH concentrations of 1×10^7 molecules cm^{-3} using 1.9 ppmv CH_4. While these estimations highlight the potential of Cl compared to OH regarding CH_4 oxidation, rigorous assessment of the impact of chlorine chemistry on a long-lived climate gas such as CH_4 requires implementing appropriate chemistry into global chemistry-transport models, which is beyond the scope of this manuscript.

6 Photolysis of HOCl as source of OH

As shown in reaction (R12), the photolysis of HOCl generates both a Cl atom and an OH radical. In the following, we compare the rates of formation of OH through the diel cycle airing from HOCl photolysis with the rate of OH formation from the photolysis of O_3 in the presence of water-vapor (R19), traditionally considered the major primary source of atmospheric OH.

$$O_3 + h\nu \rightarrow O(^1D) + O_2 \quad \text{(R19a)}$$

$$O(^1D) + H_2O \rightarrow 2OH \quad \text{(R19b)}$$

The primary photochemical production rate of OH from O_3, $P_{O_3}(OH)$ was calculated from the O_3 photolysis frequency $J_{O(^1D)}$ modified using the rate coefficients for the $O(^1D)$ reaction with H_2O or quenching by N_2 and O_2 in eqn (4). Rate coefficients k were taken from the IUPAC evaluation.[34]

$$P_{O_3}(OH) = \frac{J_{O_3(^1D)}[O_3] \times 2k_{O(^1D)+H_2O}}{k_{O(^1D)+H_2O}[H_2O] + k_{O(^1D)+N_2}[N_2] + k_{O(^1D)+O_2}[O_2]} \quad (4)$$

The diurnal cycle of the Cl and OH production rates during the "marine-anthropogenic" and "continental-unpolluted" periods (Fig. 7) show that for both periods the OH production from O_3 reaches a maximum of $\sim 7 \times 10^6$ molecules cm^{-3} s^{-1} around 13 : 00. For comparison, the maximum Cl (and thus OH from photolysis of HOCl) production rate is a factor of seven lower for the "marine-anthropogenic" case (Fig. 7a) and a factor 40 smaller for the "continental-unpolluted" case (Fig. 7b). However, in the early morning, in marine-anthropogenically influenced air the Cl production rate is more rapid than that of OH, which results from the red-shifted absorption spectra of Cl_2, HOCl and $ClNO_2$ compared to O_3 and thus better overlap with the early morning actinic flux (Fig. 7a). This is entirely consistent with the findings of Phillips *et al.*[13] at a measurement site 40 km away from our site when marine-influenced air was encountered. In this early morning period, the generation of Cl atoms results in the oxidation of hydrocarbons and thus increases the rate of formation of organic peroxyl radicals that play an important role in daytime, photochemical ozone formation.

Tropospheric OH formation occurs *via* primary formation from O_3 photolysis as well as by recycling through reaction of HO_2 with NO and (generally less importantly) the photolysis of peroxides and HONO.[101,102] HOCl is generally not considered as a potential contributor to OH production due to a lack of HOCl data. However, Fig. 9a shows that while OH formation from photolysis of O_3 is dominant, OH formation from HOCl (compare eqn (3)) is still significant at some times of the day when the actinic flux at the shorter wavelengths needed to

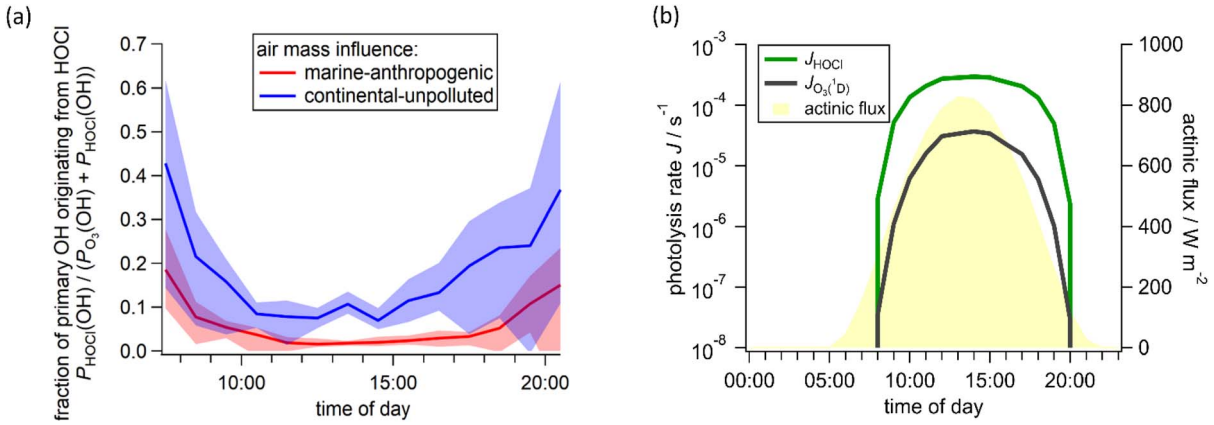

Fig. 9 The median fraction of primary OH originating from HOCl for both marine-anthropogenic and continental-unpolluted air masses (a). The actinic flux (yellow) and photolysis rates of HOCl (J_{HOCl}, green) and O_3 ($J_{O_3\ (^1D)}$, grey) (b).

photolyze O_3 is relatively weak (see Fig. 9b). For marine-anthropogenically influenced air masses, the contribution of HOCl photolysis to OH formation approaches 40% at sunrise and sunset, compared to 8% at noon. For the "continental-unpolluted" air masses, the contribution of HOCl to OH ranges from 2% at noon to 17% at sunrise and sunset. This analysis shows that HOCl should be considered as a source of primary OH formation, especially during the morning and the evening hours.

7 Conclusions

Several inorganic chlorine species (Cl_2, HOCl, $ClNO_2$ and $ClONO_2$) were measured with an Iodide-CIMS at a continental measurement site in rural central Germany, ~400 km from the nearest coastline. The largest mixing ratios were detected when 48 h-backward trajectories indicated that the air mass had passed over marine and polluted regions. The dominant chlorine-containing trace gases were $ClNO_2$ during the night and early-morning and HOCl throughout the day. A consistent feature of the $ClNO_2$ diel profile was an early morning peak, which was associated with vertical mixing. In unpolluted air, the levels of HOCl and Cl_2 were strongly enhanced compared to $ClNO_2$, while $ClONO_2$ was not observed.

In air masses with marine-anthropogenic influence we observed not only $ClNO_2$ but also $ClONO_2$ along with enhanced particulate chlorine during the nighttime. $ClONO_2$ was thus observed for the first time in tropospheric air masses, albeit at low mixing ratios of 2–3 pptv. Laboratory experiments helped rule out that this observation was not an artefact resulting, *e.g.*, from reaction of $ClNO_2$ with IO_x^- in the IMR of the instrument. Calculations of the total chlorine production rate from the photolysis of the observed species reveal values of 1.0×10^6 atoms cm^{-3} s^{-1} for air masses with marine polluted source regions, and 1.6×10^5 atoms cm^{-3} s^{-1} for continental clean ones. Depending on the air mass source region, $ClNO_2$ contributed 30–90% to Cl atom production up to three hours after sunrise and 5–10% throughout the rest of the day. Additionally, throughout the day, HOCl contributed 10–85% to Cl production, while Cl_2 was responsible for 5–20%.

Cl formation contributed significantly to radical generation (and thus oxidation rates) in the early morning implying significant peroxyl radical and ClO formation rates. The formation of OH radicals from photolysis of HOCl was compared to that by photolysis of O_3 and shown to make a significant contribution for air masses that had passed over maritime and polluted regions before reaching the site with a maximum contribution of 40% of the total primary OH formation at sunrise and sunset.

Consequentially, we show that N_2O_5-induced activation of chlorine from its particle reservoir into photolabile, gas phase forms has repercussions for the lifetimes of many hydrocarbons, highlighting methane in remote continental areas distant to source regions where it affects local chemical processes.

Author contributions

L. M. performed CIMS measurements, trajectory calculation, analyzed the data and drafted the manuscript. F. F. and F. D. performed ground-based measurements with the MoLa and data post-processing. J. N. C. performed CRDS, TD-CRDS and FT-IR measurements, synthesized the $ClONO_2$ and helped with calibration. All authors discussed the data and the presented results. All co-authors commented on the manuscript.

Conflicts of interest

There are no conflicts to declare.

Data availability

The data supporting this article have been included as part of the supplementary information (SI). Supplementary information: discussions regarding secondary ion chemistry and supporting figures. See DOI: https://doi.org/10.1039/d5ea00142k.

Data for this article, including data from all figures are available at Zenodo at https://doi.org/10.5281/zenodo.18670872.

Acknowledgements

This work was supported by internal funding from the Max Planck Society. L. M. is funded by the Deutsche Forschungsgemeinschaft (DFG, German Research Foundation)–TRR 301 "TPChange" (Project-ID 428312742). The authors thank Thomas Böttger and Philipp Schuhmann for support during the BISTUM24 campaign, and Laura Wüst for preparation of N_2O_5 crystals (all Max-Planck-Institute for Chemistry). Additionally, the authors thank Yijing Chen (Tsinghua University), Lewis Marden and Jake Willow (both from University of York), Cheng Wu (University of Gothenburg) and Cora Young (York University) for discussions about secondary ion chemistry. Open Access funding provided by the Max Planck Society.

References

1 M. J. Molina and F. S. Rowland, *Nature*, 1974, **249**, 810–812.
2 F. S. Rowland, *Environ. Conserv.*, 1988, **15**, 101–115.
3 S. Solomon, *Rev. Geophys.*, 1999, **37**, 275–316.
4 J. W. Elkins, T. M. Thompson, T. H. Swanson, J. H. Butler, B. D. Hall, S. O. Cummings, D. A. Fishers and A. G. Raffo, *Nature*, 1993, **364**, 780–783.
5 A. Engel, U. Schmidt and D. McKenna, *Geophys. Res. Lett.*, 1998, **25**, 3319–3322.
6 R. G. Prinn, R. F. Weiss, P. J. Fraser, P. G. Simmonds, D. M. Cunnold, F. N. Alyea, S. O'Doherty, P. Salameh, B. R. Miller, J. Huang, R. H. J. Wang, D. E. Hartley, C. Harth, L. P. Steele, G. Sturrock, P. M. Midgley and A. McCulloch, *J. Geophys. Res. Atmos.*, 2000, **105**, 17751–17792.
7 A. Engel, M. Strunk, M. Müller, H.-P. Haase, C. Poss, I. Levin and U. Schmidt, *J. Geophys. Res. Atmos.*, 2002, **25**(17), 3319–3322.
8 M. K. W. Ko and N. D. Sze, *J. Geophys. Res. Atmos.*, 1984, **89**, 11619–11632.
9 T. Von Clarmann and S. Johansson, *Atmos. Chem. Phys.*, 2018, **18**, 15363–15386.
10 J. A. Thornton, J. P. Kercher, T. P. Riedel, N. L. Wagner, J. Cozic, J. S. Holloway, W. P. Dubé, G. M. Wolfe, P. K. Quinn, A. M. Middlebrook, B. Alexander and S. S. Brown, *Nature*, 2010, **464**, 271–274.
11 M. J. Lawler, R. Sander, L. J. Carpenter, J. D. Lee, R. Von Glasow, R. Sommariva and E. S. Saltzman, *Atmos. Chem. Phys.*, 2011, **11**, 7617–7628.
12 L. H. Mielke, A. Furgeson and H. D. Osthoff, *Environ. Sci. Technol.*, 2011, **45**, 8889–8896.
13 G. J. Phillips, M. J. Tang, J. Thieser, B. Brickwedde, G. Schuster, B. Bohn, J. Lelieveld and J. N. Crowley, *Geophys. Res. Lett.*, 2012, **39**, L10811.
14 T. J. Bannan, A. M. Booth, A. Bacak, J. B. A. Muller, K. E. Leather, M. Le Breton, B. Jones, D. Young, H. Coe, J. Allan, S. Visser, J. G. Slowik, M. Furger, A. S. H. Prévôt, J. Lee, R. E. Dunmore, J. R. Hopkins, J. F. Hamilton, A. C. Lewis, L. K. Whalley, T. Sharp, D. Stone, D. E. Heard, Z. L. Fleming, R. Leigh, D. E. Shallcross and C. J. Percival, *J. Geophys. Res. Atmos.*, 2015, **120**, 5638–5657.
15 T. P. Marcy, R. S. Gao, M. J. Northway, P. J. Popp, H. Stark and D. W. Fahey, *Int. J. Mass Spectrom.*, 2005, **243**, 63–70.
16 M. Von Hobe, J. U. Grooß, R. Müller, S. Hrechanyy, U. Winkler and F. Stroh, *Atmos. Chem. Phys.*, 2005, **5**, 693–702.
17 R. Atkinson, D. L. Baulch, R. A. Cox, J. N. Crowley, R. F. Hampson, R. G. Hynes, M. E. Jenkin, M. J. Rossi and J. Troe, *Atmos. Chem. Phys.*, 2007, **7**, 981–1191.
18 R. Sander and P. J. Crutzen, *J. Geophys. Res. Atmos.*, 1996, **101**, 9121–9138.
19 R. von Glasow and P. J. Crutzen, in *Treatise on Geochemistry*, ed. H. D. Holland and K. K. Turekian, Pergamon, Oxford, 2003, pp. 1–67, DOI: 10.1016/B0-08-043751-6/04141-4.
20 C. Arsene, A. Bougiatioti, M. Kanakidou, B. Bonsang and N. Mihalopoulos, *Atmos. Chem. Phys.*, 2007, **7**, 4661–4673.
21 R. Von Glasow, R. Sander, A. Bott and P. J. Crutzen, *J. Geophys. Res. Atmos.*, 2002, **107**(D17), ACH 9.
22 C. Faxon, J. Bean and L. Ruiz, *Atmosphere*, 2015, **6**, 1487–1506.
23 N. Bhattacharyya, M. Modi, L. G. Jahn and L. Hildebrandt Ruiz, *Environ. Sci.: Atmos.*, 2023, **3**, 1174–1185.
24 Q. Li, D. Meidan, P. Hess, J. A. Añel, C. A. Cuevas, S. Doney, R. P. Fernandez, M. van Herpen, L. Höglund-Isaksson, M. S. Johnson, D. E. Kinnison, J.-F. Lamarque, T. Röckmann, N. M. Mahowald, A. Saiz-Lopez, Q. Li, D. Meidan, P. Hess, J. A. Añel, C. A. Cuevas, S. Doney, R. P. Fernandez, M. van Herpen, L. Höglund-Isaksson, M. S. Johnson, D. E. Kinnison, J.-F. Lamarque, T. Röckmann, N. M. Mahowald and A. Saiz-Lopez, *Nat. Commun.*, 2023, **14**(1), 4045.
25 X. Wang, D. J. Jacob, S. D. Eastham, M. P. Sulprizio, L. Zhu, Q. Chen, B. Alexander, T. Sherwen, M. J. Evans, B. H. Lee, J. D. Haskins, F. D. Lopez-Hilfiker, J. A. Thornton, G. L. Huey and H. Liao, *Atmos. Chem. Phys.*, 2019, **19**, 3981–4003.
26 W. C. Keene, A. A. P. Pszenny, D. J. Jacob, R. A. Duce, J. N. Galloway, J. J. Schultz-Tokos, H. Sievering and J. F. Boatman, *Global Biogeochem. Cycles*, 1990, **4**, 407–430.
27 W. C. Keene, R. Sander, A. A. P. Pszenny, R. Vogt, P. J. Crutzen and J. N. Galloway, *J. Aerosol Sci.*, 1998, **29**, 339–356.
28 C. Volpe, M. Wahlen, A. A. P. Pszenny and A. J. Spivack, *Geophys. Res. Lett.*, 1998, **25**, 3831–3834.
29 T. A. Cahill, K. Wilkinson and R. Schnell, *J. Geophys. Res. Atmos.*, 1992, **97**(D13), 14513–14520.
30 K. W. Oum, M. J. Lakin, D. O. DeHaan, T. Brauers and B. J. Finlayson-Pitts, *Science*, 1998, 279.
31 J. M. Lobert, W. C. Keene, J. A. Logan and R. Yevich, *J. Geophys. Res. Atmos.*, 1999, **104**, 8373–8389.
32 T. J. Bannan, M. A. H. Khan, M. Le Breton, M. Priestley, S. D. Worrall, A. Bacak, N. A. Marsden, D. Lowe, J. Pitt, G. Allen, D. Topping, H. Coe, G. McFiggans, D. E. Shallcross and C. J. Percival, *Geophys. Res. Lett.*, 2019, **46**, 8508–8516.
33 C. G. Masoud, M. Modi, N. Bhattacharyya, L. G. Jahn, K. N. McPherson, P. Abue, K. Patel, D. T. Allen and

L. Hildebrandt Ruiz, *Environ. Sci. Technol.*, 2023, **57**, 15454–15464.
34 M. Ammann, R. A. Cox, J. N. Crowley, H. Herrmann, M. E. Jenkin, V. F. McNeill, A. Mellouki, M. J. Rossi, J. Troe and T. J. Wallington, Evaluated Kinetic and Photochemical Data Foratmospheric Chemistry, 2025, https://iupac.aeris-data.fr/.
35 S. S. Brown and J. Stutz, *Chem. Soc. Rev.*, 2012, **41**, 6405.
36 J. Liebmann, E. Karu, N. Sobanski, J. Schuladen, M. Ehn, S. Schallhart, L. Quéléver, H. Hellen, H. Hakola, T. Hoffmann, J. Williams, H. Fischer, J. Lelieveld and J. N. Crowley, *Atmos. Chem. Phys.*, 2018, **18**, 3799–3815.
37 P. Dewald, T. Seubert, S. T. Andersen, G. N. T. E. Türk, J. Schuladen, M. R. McGillen, C. Denjean, J.-C. Etienne, O. Garrouste, M. Jamar, S. Harb, M. Cirtog, V. Michoud, M. Cazaunau, A. Bergé, C. Cantrell, S. Dusanter, B. Picquet-Varrault, A. Kukui, C. Xue, A. Mellouki, J. Lelieveld and J. N. Crowley, *Atmos. Chem. Phys.*, 2024, **24**, 8983–8997.
38 X. Wang, H. Wang, L. Xue, T. Wang, L. Wang, R. Gu, W. Wang, Y. J. Tham, Z. Wang, L. Yang, J. Chen and W. Wang, *Atmos. Environ.*, 2017, **156**, 125–134.
39 M. Priestley, M. Le Breton, T. J. Bannan, S. D. Worrall, A. Bacak, A. R. D. Smedley, E. Reyes-Villegas, A. Mehra, J. Allan, A. R. Webb, D. E. Shallcross, H. Coe and C. J. Percival, *Atmos. Chem. Phys.*, 2018, **18**, 13481–13493.
40 J. D. Haskins, B. H. Lee, F. D. Lopez-Hilifiker, Q. Peng, L. Jaeglé, J. M. Reeves, J. C. Schroder, P. Campuzano-Jost, D. Fibiger, E. E. McDuffie, J. L. Jiménez, S. S. Brown and J. A. Thornton, *J. Geophys. Res. Atmos.*, 2019, **124**, 8851–8869.
41 G. Chen, X. Fan, H. Wang, Y. J. Tham, Z. Lin, X. Ji, L. Xu, B. Hu and J. Chen, *Atmos. Chem. Phys.*, 2025, **25**, 7815–7828.
42 F. Schweitzer, P. Mirabel and C. George, *J. Phys. Chem. A*, 1998, **102**, 3942–3952.
43 B. J. Finlayson-Pitts, M. J. Ezell and J. N. Pitts, *Nature*, 1989, **337**, 241–244.
44 M.-T. Leu, R. S. Timonen, L. F. Keyser and Y. L. Yung, *J. Phys. Chem.*, 1995, **99**, 13203–13212.
45 G. J. Phillips, J. Thieser, M. Tang, N. Sobanski, G. Schuster, J. Fachinger, F. Drewnick, S. Borrmann, H. Bingemer, J. Lelieveld and J. N. Crowley, *Atmos. Chem. Phys.*, 2016, **16**, 13231–13249.
46 J. A. Ganske, M. J. Ezell, H. N. Berko and B. J. Finlayson-Pitts, *Chem. Phys. Lett.*, 1991, **179**, 204–210.
47 X. Peng, T. Wang, W. Wang, A. R. Ravishankara, C. George, M. Xia, M. Cai, Q. Li, C. M. Salvador, C. Lau, X. Lyu, C. N. Poon, A. Mellouki, Y. Mu, M. Hallquist, A. Saiz-Lopez, H. Guo, H. Herrmann, C. Yu, J. Dai, Y. Wang, X. Wang, A. Yu, K. Leung, S. Lee and J. Chen, *Nat. Commun.*, 2022, **13**, 939.
48 G. Chen, X. Fan, S. Yu, Y. J. Tham, Z. Lin, X. Ji, L. Xu and J. Chen, *Environ. Sci. Technol.*, 2025, **59**(10), 5164–5171.
49 M. Eigen and K. Kustin, *J. Am. Chem. Soc.*, 1962, **84**, 1355–1361.
50 G. Deiber, C. George, S. Le Calvé, F. Schweitzer and P. Mirabel, *Atmos. Chem. Phys.*, 2004, **4**, 1291–1299.
51 M. A. Tolbert, M. J. Rossi, R. Malhotra and D. M. Golden, *Science*, 1987, **238**, 1258–1260.
52 R. J. Cicerone, *Rev. Geophys.*, 1981, **19**, 123–139.
53 T. E. Caldwell, K. L. Foster, T. Benter, S. Langer, J. C. Hemminger and B. J. Finlayson-Pitts, *J. Phys. Chem. A*, 1999, **103**, 8231–8238.
54 J. P. Kercher, T. P. Riedel and J. A. Thornton, *Atmos. Meas. Tech.*, 2009, **2**, 193–204.
55 B. H. Lee, F. D. Lopez-Hilfiker, C. Mohr, T. Kurtén, D. R. Worsnop and J. A. Thornton, *Environ. Sci. Technol.*, 2014, **48**, 6309–6317.
56 D. Maric, J. P. Burrows, R. Meller and G. K. Moortgat, *J. Photochem. Photobiol., A*, 1993, **70**, 205–214.
57 J. A. Davidson, C. A. Cantrell, R. E. Shetter, A. H. McDaniel and J. G. Calvert, *J. Geophys. Res. Atmos.*, 1987, **92**, 10921–10925.
58 N. Sobanski, J. Schuladen, G. Schuster, J. Lelieveld and J. N. Crowley, *Atmos. Meas. Tech.*, 2016, **9**, 5103–5118.
59 Y. Ji, L. G. Huey, D. J. Tanner, Y. R. Lee, P. R. Veres, J. A. Neuman, Y. Wang and X. Wang, *Atmos. Meas. Tech.*, 2020, **13**, 3683–3696.
60 J. Thieser, G. Schuster, J. Schuladen, G. J. Phillips, A. Reiffs, U. Parchatka, D. Pöhler, J. Lelieveld and J. N. Crowley, *Atmos. Meas. Tech.*, 2016, **9**, 553–576.
61 J. A. Davidson, A. A. Viggiano, C. J. Howard, I. Dotan, F. C. Fehsenfeld, D. L. Albritton and E. E. Ferguson, *J. Chem. Phys.*, 1978, **68**, 2085–2087.
62 J. M. Roberts, H. D. Osthoff, S. S. Brown, A. R. Ravishankara, D. Coffman, P. Quinn and T. Bates, *Geophys. Res. Lett.*, 2009, **36**, L20808.
63 F. Drewnick, T. Böttger, S. L. von der Weiden-Reinmüller, S. R. Zorn, T. Klimach, J. Schneider and S. Borrmann, *Atmos. Meas. Tech.*, 2012, **5**, 1443–1457.
64 J. Pikmann, F. Drewnick, F. Fachinger and S. Borrmann, *Atmos. Chem. Phys.*, 2024, **24**, 12295–12321.
65 G. C. Roberts, M. V. Ramana, C. Corrigan, D. Kim and V. Ramanathan, *Proc. Natl. Acad. Sci. U. S. A.*, 2008, **105**, 7370–7375.
66 A. F. Stein, R. R. Draxler, G. D. Rolph, B. J. B. Stunder, M. D. Cohen and F. Ngan, *Bull. Am. Meteorol. Soc.*, 2015, **96**, 2059–2077.
67 G. Rolph, A. Stein and B. Stunder, *Environ. Model. Software*, 2017, **95**, 210–228.
68 Y. J. Tham, C. Yan, L. Xue, Q. Zha, X. Wang and T. Wang, *Chin. Sci. Bull.*, 2014, **59**, 356–359.
69 T. P. Riedel, G. M. Wolfe, K. T. Danas, J. B. Gilman, W. C. Kuster, D. M. Bon, A. Vlasenko, S. M. Li, E. J. Williams, B. M. Lerner, P. R. Veres, J. M. Roberts, J. S. Holloway, B. Lefer, S. S. Brown and J. A. Thornton, *Atmos. Chem. Phys.*, 2014, **14**, 3789–3800.
70 B. D. Finley and E. S. Saltzman, *Geophys. Res. Lett.*, 2006, **33**, L11809.
71 A. A. P. Pszenny, W. C. Keene, D. J. Jacob, S. Fan, J. R. Maben, M. P. Zetwo, M. Springer-Young and J. N. Galloway, *Geophys. Res. Lett.*, 1993, **20**, 699–702.
72 C. W. Spicer, E. G. Chapman, B. J. Finlayson-Pitts, R. A. Plastridge, J. M. Hubbe, J. D. Fast and C. M. Berkowitz, *Nature*, 1998, **394**, 353–356.

73 X. Chen, Y. Jiang, Z. Zong, Y. Wang, W. Sun, Y. Wang, M. Xia, L. Guan, P. Liu, C. Zhang, J. Chen, Y. Mu and T. Wang, *Environ. Sci. Technol.*, 2025, **59**, 12775–12785.
74 H. D. Osthoff, J. M. Roberts, A. R. Ravishankara, E. J. Williams, B. M. Lerner, R. Sommariva, T. S. Bates, D. Coffman, P. K. Quinn, J. E. Dibb, H. Stark, J. B. Burkholder, R. K. Talukdar, J. Meagher, F. C. Fehsenfeld and S. S. Brown, *Nat. Geosci.*, 2008, **1**, 324–328.
75 M. Le Breton, Å. M. Hallquist, R. K. Pathak, D. Simpson, Y. Wang, J. Johansson, J. Zheng, Y. Yang, D. Shang, H. Wang, Q. Liu, C. Chan, T. Wang, T. J. Bannan, M. Priestley, C. J. Percival, D. E. Shallcross, K. Lu, S. Guo, M. Hu and M. Hallquist, *Atmos. Chem. Phys.*, 2018, **18**, 13013–13030.
76 J. Zhang and D. Kinnison, TUV Calculator, NCAR (National Center for Atmospheric Research), Boulder, Colorado, 2025, https://www.acom.ucar.edu/Models/TUV/Interactive_TUV/, accessed 15.06.2025.
77 T. H. Bertram and J. A. Thornton, *Atmos. Chem. Phys.*, 2009, **9**, 8351–8363.
78 S. R. Zorn, F. Drewnick, M. Schott, T. Hoffmann and S. Borrmann, *Atmos. Chem. Phys.*, 2008, **8**, 4711–4728.
79 L. Moormann, F. Fachinger, F. Drewnick and H. Tost, *EGUsphere*, 2025, pp. 1–23, DOI: 10.5194/egusphere-2025-3862.
80 J. N. Crowley, G. Schuster, N. Pouvesle, U. Parchatka, H. Fischer, B. Bonn, H. Bingemer and J. Lelieveld, *Atmos. Chem. Phys.*, 2010, **10**, 2795–2812.
81 Y. Ge, S. Solberg, M. R. Heal, S. Reimann, W. Van Caspel, B. Hellack, T. Salameh and D. Simpson, *Atmos. Chem. Phys.*, 2024, **24**, 7699–7729.
82 M. Ragains and B. Finlayson-Pitts, *J. Phys. Chem. A*, 1997, **101**, 1509–1517.
83 J. Burkholder, S. Sander, J. Abbatt, J. Barker, C. Cappa, J. Crounse, T. Dibble, R. Huie, C. Kolb and M. Kurylo, *Chemical Kinetics and Photochemical Data for Use in Atmospheric Studies; Evaluation Number 19*, Jet Propulsion Laboratory, National Aeronautics and Space, Pasadena, CA, 2020.
84 J. D. Haskins, L. Jaeglé, V. Shah, B. H. Lee, F. D. Lopez-Hilfiker, P. Campuzano-Jost, J. C. Schroder, D. A. Day, H. Guo, A. P. Sullivan, R. Weber, J. Dibb, T. Campos, J. L. Jimenez, S. S. Brown and J. A. Thornton, *J. Geophys. Res. Atmos.*, 2018, **123**, 12897–12916.
85 A. A. Angelucci, T. C. Furlani, X. Wang, D. J. Jacob, T. C. Vandenboer and C. J. Young, *ACS Earth Space Chem.*, 2021, **5**, 2507–2516.
86 R. Atkinson, S. M. Aschmann, J. Arey and B. Shorees, *J. Geophys. Res. Atmos.*, 1992, **97**, 6065–6073.
87 R. A. Cox, M. Ammann, J. N. Crowley, H. Herrmann, M. E. Jenkin, V. F. McNeill, A. Mellouki, J. Troe and T. J. Wallington, *Atmos. Chem. Phys.*, 2020, **20**, 13497–13519.
88 I. Bey, B. Aumont and G. Toupance, *Geophys. Res. Lett.*, 1997, **24**, 1067–1070.
89 I. Faloona, D. Tan, W. Brune, J. Hurst, D. Barket, T. L. Couch, P. Shepson, E. Apel, D. Riemer, T. Thornberry, M. A. Carroll, S. Sillman, G. J. Keeler, J. Sagady, D. Hooper and K. Paterson, *J. Geophys. Res. Atmos.*, 2001, **106**, 24315–24333.
90 X. Ren, H. Harder, M. Martinez, R. L. Lesher, A. Oliger, J. B. Simpas, W. H. Brune, J. J. Schwab, K. L. Demerjian, Y. He, X. Zhou and H. Gao, *Atmos. Environ.*, 2003, **37**, 3639–3651.
91 M. A. H. Khan, M. J. Ashfold, G. Nickless, D. Martin, L. A. Watson, P. D. Hamer, R. P. Wayne, C. E. Canosa-Mas and D. E. Shallcross, *Atmos. Sci. Lett.*, 2008, **9**, 140–146.
92 R. L. Caravan, M. F. Vansco and M. I. Lester, *Commun. Chem.*, 2021, **4**, 44.
93 H. Wang and Y.-P. Lee, *J. Phys. Chem. A*, 2024, **128**, 8690–8698.
94 T. H. Bertram, J. A. Thornton, T. P. Riedel, A. M. Middlebrook, R. Bahreini, T. S. Bates, P. K. Quinn and D. J. Coffman, *Geophys. Res. Lett.*, 2009, **36**, L19803.
95 M. Xia, X. Peng, W. Wang, C. Yu, P. Sun, Y. Li, Y. Liu, Z. Xu, Z. Wang, Z. Xu, W. Nie, A. Ding and T. Wang, *Atmos. Chem. Phys.*, 2020, **20**, 6147–6158.
96 Y. Li, W. Nie, Y. Liu, D. Huang, Z. Xu, X. Peng, C. George, C. Yan, Y. J. Tham, C. Yu, M. Xia, X. Fu, X. Wang, L. Xue, Z. Wang, Z. Xu, X. Chi, T. Wang and A. Ding, *Environ. Sci. Technol. Lett.*, 2020, **7**, 70–75.
97 E. Z. Dalton, E. H. Hoffmann, T. Schaefer, A. Tilgner, H. Herrmann and J. D. Raff, *J. Am. Chem. Soc.*, 2023, **145**, 15652–15657.
98 G. Chen, L. Xu, S. Yu, L. Xue, Z. Lin, C. Yang, X. Ji, X. Fan, Y. J. Tham, H. Wang, Y. Hong, M. Li, J. H. Seinfeld and J. Chen, *Environ. Sci. Technol.*, 2024, **58**, 22714–22721.
99 J. Dai, T. Wang, H. Shen, M. Xia, W. Sun and G. P. Brasseur, *Environ. Sci. Technol.*, 2025, **59**, 2169–2180.
100 T. P. Riedel, T. H. Bertram, T. A. Crisp, E. J. Williams, B. M. Lerner, A. Vlasenko, S.-M. Li, J. Gilman, J. de Gouw, D. M. Bon, N. L. Wagner, S. S. Brown and J. A. Thornton, *Environ. Sci. Technol.*, 2012, **46**, 10463–10470.
101 J. Lelieveld, F. J. Dentener, W. Peters and M. C. Krol, *Atmos. Chem. Phys.*, 2004, **4**, 2337–2344.
102 G. Chua, V. Naik and L. W. Horowitz, *Atmos. Chem. Phys.*, 2023, **23**, 4955–4975.